Journal of Structural Geology 33 (2011) 713–730

Contents lists available at ScienceDirect

Journal of Structural Geology

journal homepage: www.elsevier.com/locate/jsg

Microstructure and crystallographic preferred orientation of polycrystalline microgarnet aggregates developed during progressive creep, recovery, and grain boundary sliding

Matthew A. Massey [a,*], David J. Prior [b], David P. Moecher [c]

[a] Massachusetts Geological Survey, University of Massachusetts, Amherst, MA 01003-9297, USA
[b] Earth & Ocean Sciences, University of Liverpool, Liverpool L69 3GP, UK
[c] Earth & Environmental Sciences, University of Kentucky Lexington, KY 40506-0053, USA

ARTICLE INFO

Article history:
Received 30 October 2009
Received in revised form
22 November 2010
Accepted 15 December 2010
Available online 23 December 2010

Keywords:
Garnet
Grain boundary sliding
Diffusion
Plastic deformation
Electron backscatter diffraction

ABSTRACT

Optical microscopy, electron probe microanalysis, and electron backscatter diffraction methods have been used to examine a broad range of garnet microstructures within a high strain zone that marks the western margin of a major transpression zone in the southern New England Appalachians. Garnet accommodated variable states of finite strain, expressed as low strain porphyroclasts (*Type 1*), high strain polycrystalline aggregates (*Type 2*), and transitional morphologies (*Type 3*) that range between these end members. *Type 1* behaved as rigid porphyroclasts and is characterized by four concentric Ca growth zones. *Type 2* help define foliation and lineation, are characterized by three Ca zones, and possess a consistent bulk crystallographic preferred orientation of (100) symmetrical to the tectonic fabric. *Type 3* show variable degrees of porphyroclast associated with aggregate, where porphyroclasts display complex compositional zoning that corresponds to lattice distortion, low-angle boundaries, and subgrains, and aggregate CPO mimics porphyroclast orientation. All aggregates accommodated a significant proportion of greenschist facies deformation through grain boundary sliding, grain rotation and impingement, and pressure solution, which lead to a cohesive behavior and overall strain hardening of the aggregates. The characteristic CPO could not have been developed in this manner, and was the result of an older phase of partitioned amphibolite facies dislocation creep, recovery including chemical segregation, and recrystallization of porphyroclasts. This study demonstrates the significance of strain accommodation within garnet and its affect on composition under a range of PT conditions, and emphasizes the importance of utilizing EBSD methods with studies that rely upon a sound understanding of garnet.

1. Introduction

Garnet has an extensive P–T stability range, is a fundamental constituent of crust and mantle lithologies, serves as a key constraint in several important thermobarometric models (Pattison and Tracy, 1991; Spear, 1992), and can be used for complex tectonic reconstructions (e.g., Spear and Selverstone, 1983; Bell and Johnson, 1989; Kohn et al., 2001; Bell and Kim, 2004). Therefore, a sound understanding of the chemical and physical behavior of garnet is essential to a range of petrotectonic applications. The complexities of garnet are exemplified by recent microstructural investigations that identified considerable intracrystalline substructure, which could not be identified with standard petrographic methods. These substructures have been variously attributed to garnet deformation by crystal plastic (Ji and Martingole, 1994; Kleinschrodt and McGrew, 2000; Kleinschrodt and Duyster, 2002; Prior et al., 2000, 2002; Storey and Prior, 2005; Bestmann et al., 2008) and cataclastic (Trepmann and Stockhert, 2002) mechanisms, as well as garnet growth from enlargement and amalgamation of multiple nuclei (Daniel and Spear, 1998; Spiess et al., 2001; Wheeler et al., 2001; Prior et al., 2002; Dobbs et al., 2003; Whitney and Seaton, 2010).

Plastic deformation and dynamic recrystallization of many minerals (e.g., quartz, calcite, and olivine) are often accompanied by the development of a strong crystallographic preferred orientation (CPO; e.g., Schmid and Casey, 1986; Mainprice and Nicolas, 1989; Rutter et al., 1994). Transmission electron microscope (TEM) studies indicate that dislocation slip occurs in

* Corresponding author. Fax: +1 413 545 1200.
E-mail address: mmassey@geo.umass.edu (M.A. Massey).

0191-8141/$ – see front matter © 2010 Elsevier Ltd. All rights reserved.
doi:10.1016/j.jsg.2010.12.009

experimentally (e.g., Voegele et al., 1998b; Li et al., 2006) and naturally (e.g., Ji and Martingole, 1994; Voegele et al., 1998a) deformed garnet. Storey and Prior (2005) and Bestmann et al. (2008) have shown that dislocation slip, recovery, and recrystallization in garnet are associated with increasing strain. Storey and Prior (2005) demonstrate that the single crystal orientation of a garnet porphyroclast becomes progressively more dispersed around a rational crystallographic axis, and then increasingly weakened toward a random orientation. They attribute this CPO evolution to increasing strain within the amphibolite facies, where the original porphyroclast initially deformed by dislocation creep and recovery, followed by subgrain rotation recrystallization, and finally grain boundary sliding. Bestmann et al. (2008) report similar findings within upper amphibolite facies garnet porphyroclasts, and Terry and Heidelbach (2004) identify eclogite facies diffusion creep as the predominant deformation mechanism within fine-grained (~10 μm) aggregates. Using experimentally determined slip systems, the numerical simulations of Mainprice et al. (2004) predict characteristic garnet CPO as an expression of specific flow regimes (axial compression, pure shear, and simple shear); however, the match between model fabrics and natural CPO's is ambiguous. Despite the evidence for CPO-producing garnet deformation mechanisms, and the theoretical basis for characteristic preferred orientations, a consistent CPO of garnet linked to deformation has yet to be presented.

This study examines garnet microstructures, which range from single crystal porphyroclasts to polycrystalline microgarnet aggregates, in the margin of a transpression zone in southern New England, U.S.A. Aggregate CPO's are consistent from sample to sample, and symmetrical to the high strain zone fabric elements, and thus appear to represent a bulk garnet CPO. We discuss the evolution of these aggregates in terms of chemical composition, microstructure, and active deformation mechanisms, and then present a conceptual model of garnet evolution.

2. Geologic setting

Episodic tectonometamorphism, spanning almost the entire Paleozoic, is responsible for the amalgamation of terranes that comprise the northern Appalachians (Robinson et al., 1998; van Staal, 2006). These terranes and zones vary in provenance, style of deformation, degree of metamorphism, and/or timing. However, the general pattern of northeast to northern strike of the orogen is the result of oblique convergence between Laurentia and outboard Avalon and Meguma terranes, which progressed from the middle to late Paleozoic throughout Maritime Canada and southeastern New England, respectively (Solar and Brown, 2001; van Staal, 2006). In southeastern New England, late Paleozoic tectonism is manifested as ductile deformation partitioned among lithologic units of varying competency, particularly terrane boundaries and metastratified rocks mantling gneiss domes (Fig. 1; e.g., Getty and Gromet, 1992; Moecher and Wintsch, 1994; Robinson et al., 1998; Moecher, 1999). The Bronson Hill zone likely represents the most inboard extent of such intense effects, where relatively thin metavolcanic and metasedimentary cover mantling elongate metaigneous bodies generated marked rheological contrasts (Massey and Moecher, 2008).

The Mt. Dumplin high strain zone (Fig. 1b) is the western boundary of a major transpression zone within the Bronson Hill zone of south-central Massachusetts (Massey and Moecher, 2008). Strain was concentrated within a narrow (~500 m) sequence of west-dipping metavolcanic and metasedimentary rocks mantling an elongate tonalitic orthogneiss body (Fig. 1b). S–C fabrics, asymmetric folds, porphyroclasts, and boudins consistently display sinistral asymmetries in planes parallel to the moderately southwest-plunging mineral stretching lineations, and commonly normal (west-side-down) asymmetries on planes orthogonal to lineation and foliation (Figs. 1c and 2). A mylonitic pelitic schist unit within the high strain zone is the host for the garnet microstructures that are the focus of this study (Fig. 2).

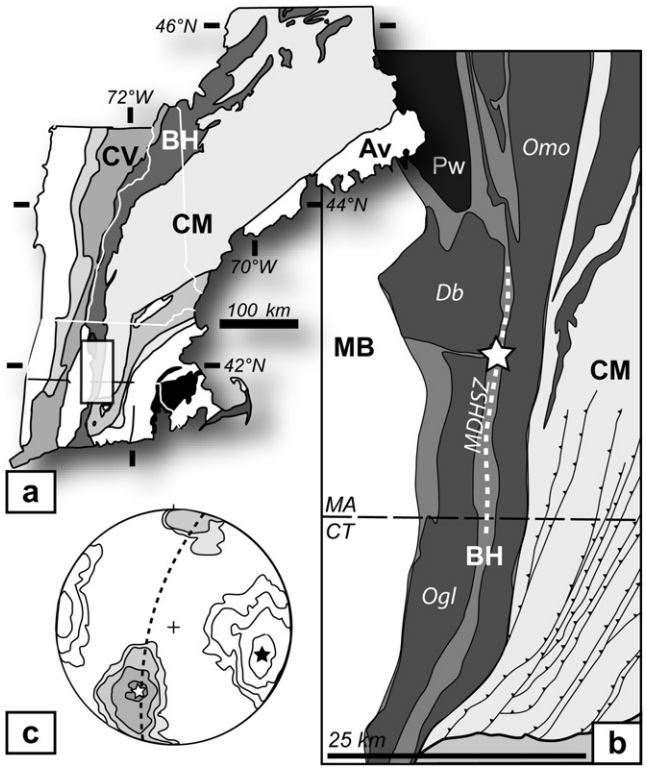

Fig. 1. (a) Lithotectonic zones of New England Appalachians. (b) Simplified geologic map of southeastern New England. Mt. Dumplin high strain zone (MDHSZ) bounds western margin of Monson gneiss (Omo). Extent of mapped garnet microstructures indicated by dashed line; location of samples used in this study shown by star. Av, Avalon terrane; BH, Bronson Hill zone; CM, Central Maine zone; CV, Connecticut Valley zone; Db, Belchertown complex; MB, Mesozoic basin; Ogl, Glastonbury gneiss; Pw, Pelham window. (c) Equal area lower hemisphere plot of MDHSZ fabric elements. Foliations contoured in white (mean = 015/74° W) and lineations contoured in gray (mean = 37°/210).

3. Analytical techniques

Semi-quantitative compositional X-ray mapping and quantitative chemical analyses of garnet microstructures were obtained by electron probe microanalysis, carried out at the University of Kentucky. Compositional X-ray mapping was performed on a ARL-SEMQ electron microprobe using a combination of beam and stage scans at an operating voltage of 15 keV, sample currents of ~60 nA, and dwell times of 0.01–0.03 s. X-ray mapping focused on the distribution of major elements Mg, Mn, and Ca, and trace elements Y, P, and Na. These elements possess varying volume diffusivities in garnet and preserve to varying degrees compositional zoning developed during stages of garnet growth. Quantitative chemical analyses of major elements in garnet were subsequently acquired using a CAMECA SX-50 with an accelerating potential of 15 keV and 20 nA sample current.

Electron backscatter diffraction (EBSD) and orientation contrast (OC) imaging were completed at the University of Liverpool. Automated EBSD mapping (e.g., Prior et al., 2002) was performed on SYTON-polished thin sections (e.g., Prior et al., 1996) using a CamScan X500 crystal probe fitted with a thermoionic field

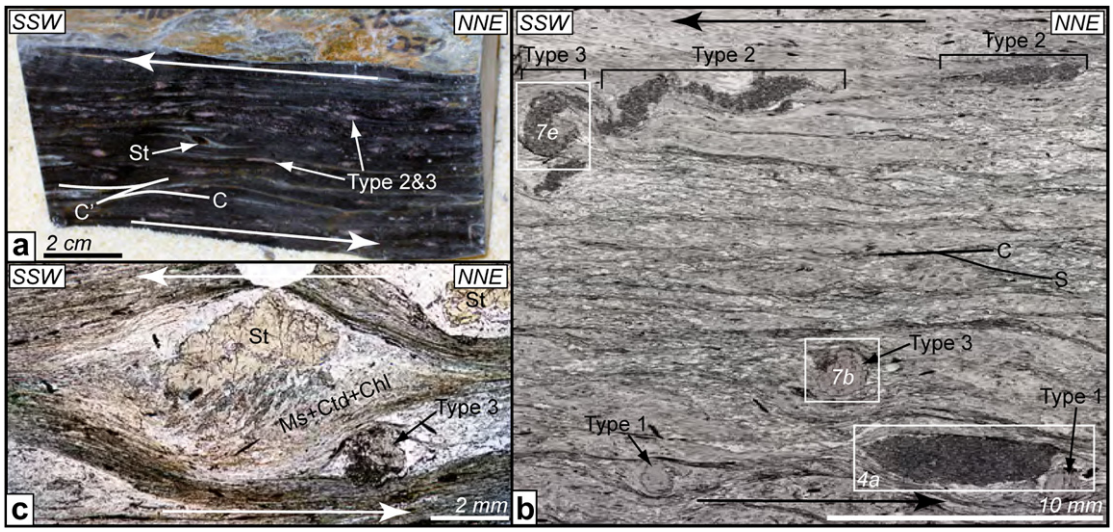

Fig. 2. MDHSZ fabrics and mineral assemblages. (a) Hand sample of garnet-bearing pelitic schist cut parallel to lineation and normal to foliation. Notice sinistral kinematics indicated by shear band (C') and asymmetric staurolite (St) porphyroclast. Pink polycrystalline layers of garnet contain *Type 2* and *3* microstructures. *Type 1* garnet porphyroclasts are dark maroon and barely visible. (b) Thin-section photograph showing three distinct garnet morphologies in close spatial proximity, and sinistral S–C fabric. Locations of Figs. 4a, 7b, and 7e are marked. (c) St porphyroclast with sinistral asymmetry partially replaced by muscovite (Ms), chloritoid (Ctd), and chlorite (Chl). (For interpretation of the references to color in this figure legend, the reader is referred to the web version of this article).

emission gun running at 20 keV with a beam current of 20 nA. Data were indexed and processed with CHANNEL 5 software using procedures outlined by Prior et al. (2002) and Bestmann and Prior (2003). Additional details of data acquisition and processing are explained below.

4. Microstructural context

The host lithology of garnet microstructures is a well-foliated, gray- to rusty-weathering Qtz + Ms + Grt + Rt + Chl ± Bt mylonitic schist (Fig. 2). The metamorphic grade of deformation is variable. The predominant stable mylonitic fabric is defined by muscovite, layers of quartz, polycrystalline garnet aggregates, minor acicular rutile, and locally biotite and/or chlorite (Fig. 2). Porphyroclasts of staurolite, garnet, and albite define a relict higher-grade (amphibolite facies) assemblage (Fig. 2) that has been overprinted by the current mylonitic fabric. Staurolite has been variably replaced by Ms + Ctd + Chl that also define sigma- and theta-type tails (Fig. 2c), albite has been variably pseudomorphed by muscovite, and sigma- and theta-type quartz tails (locally with minor Chl) are associated with garnet porphyroclasts (Fig. 2b). The local presence of chlorite associated with staurolite and garnet porphyroclasts suggests some greenschist facies deformation (Fig. 2c). Thermobarometric calculations along strike of the study area place conditions of peak staurolite-grade metamorphism at 625° and 9 kbar to the south (Berg and Moecher, 2005), and 550° and 6 kbar to the north (e.g., Spear et al., 2002).

Three types of garnet microstructures can be distinguished optically (Fig. 2b): (*Type 1*) coarse-grained garnet porphyroclasts; (*Type 2*) aggregates of fine-grained garnet crystals; (*Type 3*) transitional morphologies. Garnet microstructures are in close proximity to one another, and we have not recognized any association to explain their spatial distribution (Fig. 2b). The primary focus of the present contribution is the deformation and fabric of *Type 2* and *3* polycrystalline garnet aggregates, however, all garnet microstructures will be introduced and discussed in order to provide a suitable context and relative timing for aggregate evolution and deformation. Although the detailed parageneses of all garnet microstructures and their relationship with the pressure–temperature–time path of the host lithology is, no doubt, important in order to fully understand the significance of *Type 2* garnet aggregates, it is beyond the scope of this study. Results of petrographic observations, X-ray mapping and quantitative analyses, and OC imaging are discussed below in order to place the garnet aggregates in their proper framework. EBSD data are then presented and discussed, along with additional X-ray maps and OC images.

4.1. *Type 1* – porphyroclasts

Type 1 microstructures consist of coarse-grained (1–2 mm) porphyroclasts, and are the least common of the three microstructural varieties. Porphyroclasts are enveloped by the foliation, commonly producing strain caps of Ms + Rt ± Chl and sigma- and theta-type tails of quartz (Fig. 3a). Very fine-grained opaque inclusions define a subhedral to euhedral core, and anhedral rim. Chlorite is locally observed within tails of garnet porphyroclasts, but significant replacement by chlorite is not observed. OC imaging does not reveal any significant internal substructure due to crystal lattice distortion (Fig. 3e).

Compositional X-ray mapping shows the distribution of Mg, P, and Na in *Type 1* porphyroclasts to be homogeneous. Four distinct compositional zones are revealed by the Ca distribution (Fig. 3b): (1) coarse-grained, euhedral Ca-enriched core; (2) thin, euhedral Ca-depleted overgrowth; (3) subhedral to euhedral Ca-enriched overgrowth; (4) anhedral to subhedral Ca-depleted rim. Y concentrations are relatively small (Fig. 3c), but zoning mimics that of Ca with a Y-enriched core and Y-depleted overgrowth (Ca zones 1 and 2, respectively). These two Y zones are overgrown by a very thin Y-enriched zone that coincides with the beginning of Ca zone 3, and a thick Y-depleted overgrowth. Mn zoning (Fig. 3d) defines an enriched core that corresponds to Ca zones 1 and 2, and Mn-depleted rim corresponding to Ca zones 3 and 4.

Quantitative point analyses taken along traverses (step size of 10 μm) across *Type 1* porphyroclasts corroborate qualitative observations. Profiles of pyrope and spessartine are consistent throughout both samples (Fig. 3f and g; also see Fig. 14). Pyrope is uniform throughout the porphyroclasts with compositions ranging from 7.3 to 7.6%, locally with slight enrichment along rims to 7.8%. Spessartine

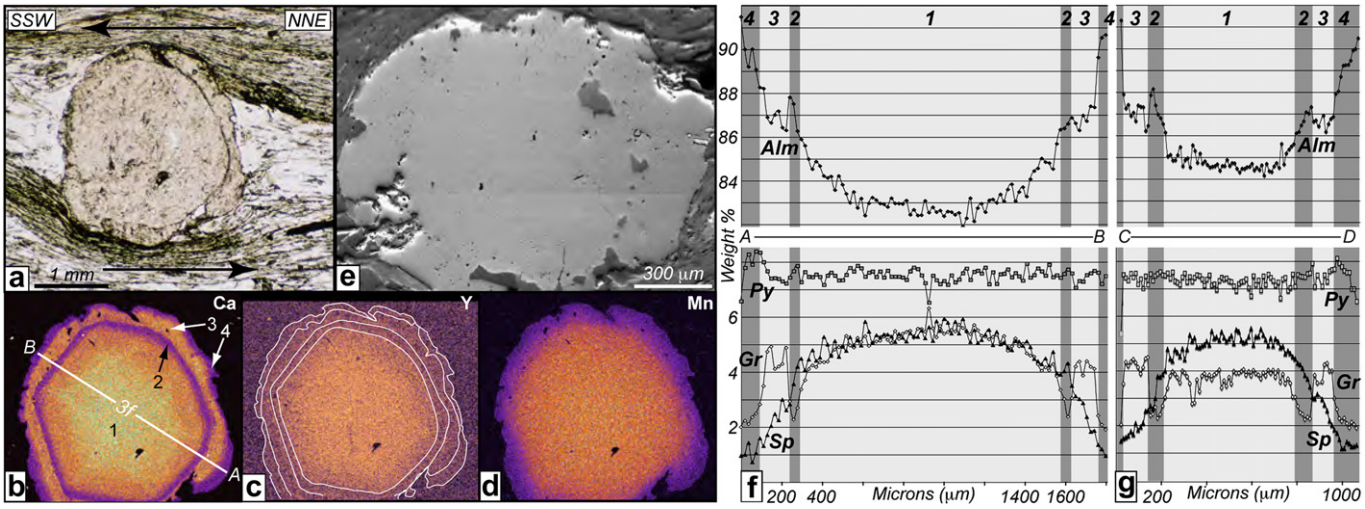

Fig. 3. *Type 1* garnet. (a) Photomicrograph of sigma-type porphyroclast. (b–d) Compositional X-ray maps showing concentric zoning of Ca (b) and Y (c), and diffuse zoning of Mn (d). Notice four zones (Ca zones 1–4) preserved by Ca. White lines in (c) mark Ca zoning, which corresponds with weak Y zoning. In all X-ray maps, increasingly bright colors indicate higher concentrations of mapped element. Line A–B marks location of microprobe traverse shown in Fig. 3f. (e) SEM OC image of *Type 1* porphyroclast (not same as shown in a–d) showing no internal crystallographic substructure or lattice distortion. (For interpretation of the references to color in this figure legend, the reader is referred to the web version of this article). (f and g) Distribution of almandine (Alm), pyrope (Py), grossular (Gr), and spessartine (Sp) components taken along microprobe traverses across *Type 1* porphyroclasts. Varying shades of gray mark "Ca zones 1-4", as identified by X-ray mapping. (f) Sample M1605-2-L3. (g) Sample M1605-2-L1.

content steadily decreases from ~5% in the cores to ~1% in the rims. Profiles of grossular confirm the four zones identified by elemental mapping, however there is some variability in composition from sample to sample. Sample M1605-2-L3 (Fig. 3f) yields grossular contents of 5.1% in Ca zone 1 (core), 3.1% in Ca zone 2 (inner overgrowth), 4.4% in Ca zone 3 (outer overgrowth), and 2.4% in the Ca zone 4 (rim). Grossular contents are somewhat lower in M1605-2-L1 (Fig. 3g) with values of 3.6%, 2.4%, 4.0%, and 2.3% from Ca zones 1 (core) to 4 (rim), respectively. Overall, almandine content increases gradually from core to rim in both samples; however, small compositional variations correspond to each of the four domains as defined by Ca/grossular (Fig. 3f and g; also see Fig. 14).

4.2. *Type 2* – aggregates

Multiple, fine-grained, micron-scale garnet crystals within a matrix of quartz comprise large aggregates and chains that help define the mylonitic foliation and lineation (Fig. 4a and b). Aspect ratios of aggregates range from 1:1 to as high as 22:1, however most are in the range of 6:1 to 12:1. These aggregates are easily identified in outcrop as pink microcrystalline layers up to several centimeters in length, and similar microstructures are observed along a 25 km strike-length within the high strain zone. Rotation of garnet layers into parallelism with mesoscopic-scale shear bands is observed locally, which further demonstrates their association with the

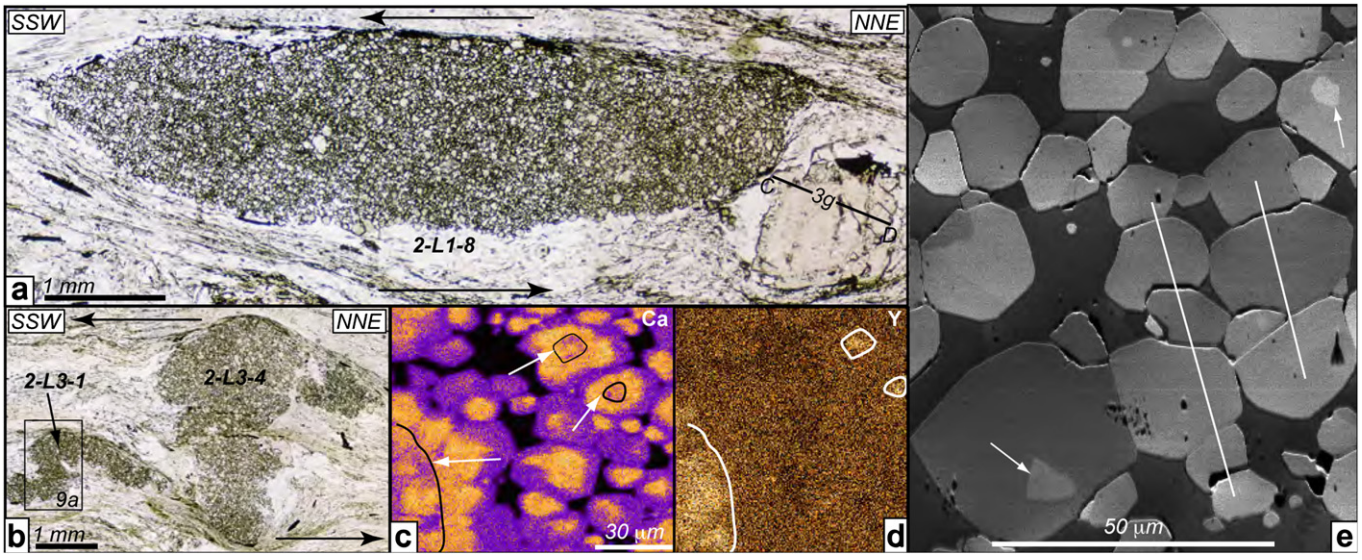

Fig. 4. *Type 2* polycrystalline aggregates. (a) Photomicrograph of sigma-type aggregate. Notice close spatial association with *Type 1* porphyroclast (Gt1). Line C–D marks location of microprobe traverse shown in Fig. 3g. (b) Photomicrograph of delta-type *Type 2* aggregate and asymmetric fold. Location of Fig. 9a shown by box. (c & d) Compositional X-ray map showing Ca (c) and Y (d) zoning within individual aggregate crystals. Notice correspondence of irregular Ca zoning in some cores (outlined in black) with Y enrichment. (e) Detailed OC image of aggregate grains (light gray with high relief) within a matrix of quartz (dark gray). Notice euhedral to subhedral, faceted, and elliptical morphologies, sub-vertical stacking and impingement of individual grains (parallel to white lines), and distinct faceted inclusions (arrows). (For interpretation of the references to color in this figure legend, the reader is referred to the web version of this article).

mylonitic fabric. Despite deformation and flow, aggregates appear to have behaved as a cohesive unit without significant phase mixing, defining pinch and swell structures, sigma- and delta-type kinematic indicators, asymmetric folds, and homogeneous layers, all consistent with sinistral and normal kinematics of the high strain zone.

OC imaging shows that individual garnet grains are commonly characterized by euhedral facet traces along quartz-garnet interfaces and gently curved to straight grain boundaries along garnet-garnet interfaces (Figs. 4e and 5). Facet trace analyses show that crystal facets are most consistent with being predominantly {112} and {110} faces, some {111} faces, and rare {100} faces (Fig. 5). {112} and {110} faces are predominant in rhombohedral or icositetrahedral garnets (Read, 1970; Deer et al., 1992). Grain shape analyses indicate that axial ratios of individual grains average ~1.55, and are inversely proportional to grain size. A range of intracrystalline substructure within aggregate garnet grains is also observed in OC images, defined by differences in crystal lattice orientations. Porphyroblasts with equant inclusional substructures (Fig. 4e), subvertical impingement and stacking of porphyroblasts (Fig. 4e), and lattice distortion and subgrain development within anhedral grains will all be presented in detail below.

X-ray mapping reveals a Ca-enriched core and Ca-depleted rim within most individual crystals, however some *Type 2* garnet crystals display slightly depleted irregular cores (Fig. 4c). Y enrichment coincides with the latter irregular Ca cores only, and is always homogeneous elsewhere in *Type 2* garnet (Fig. 4d). Quantitative point analyses performed on cores of random faceted grains within sample M1605-2-L1 (Fig. 6) indicate rather uniform compositions of almandine, pyrope, and spessartine, with ranges of 86.9–89.7% (mean = 88.1%), 6.7–8.1% (mean = 7.4%), and 1.0–1.5% (mean = 1.2%), respectively. However, grossular contents show considerable variation in the range of 1.9%–4.3%. The range of grossular content in garnet from *Type 2* microstructures is the same as that of all four Ca zones in the *Type 1* porphyroclast from the same sample (see Fig. 3g); however, this point will be discussed later.

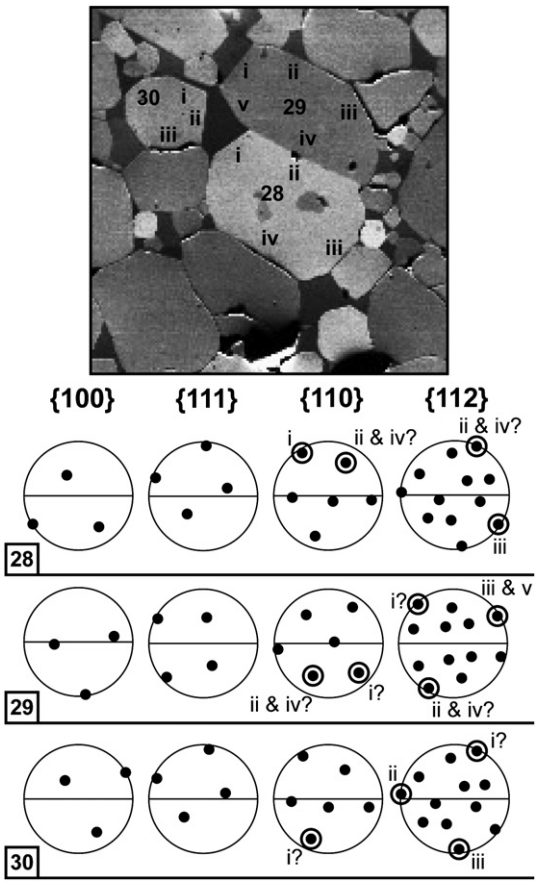

Fig. 5. Facet trace analyses of three grains (28, 29, and 30) shown in OC image (top). Stereonets show the {100}, {110}, {111}, and {112} single crystal orientations of each numbered grain. Crystal directions that are circled could correspond to poles to facet planes marked by roman numerals in OC image.

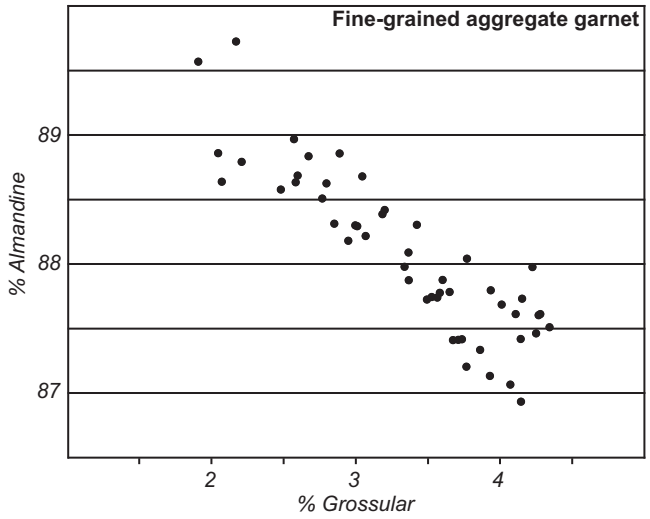

Fig. 6. Plot of grossular vs. almandine point analyses taken from cores of individual aggregate garnet grains in sample M1605-2-L1. Notice the lack of any separation of distinct compositional zones.

4.3. *Type 3 – transitions*

Optically, *Type 3* microstructures are characterized by variable proportions of relicts of *Type 1* porphyroclast and *Type 2* aggregate, which creates the appearance of a transitional state between these end members (Fig. 7). The location of some *Type 3* microstructures within long boudinaged layers of fine-grained garnet, can make the distinction between *Type 2* and *Type 3* microstructures one of scale (Fig. 7a). Coarse-grained relicts similar to *Type 1* are variable in size, morphology, and spatial distribution within the aggregate. In general, as aggregate volume increases, millimeter-scale euhedral to subhedral relicts progress to micron-scale anhedral fragments scattered throughout the aggregate. *Type 3* transitional microstructures commonly display both sigma- and delta-type asymmetries (Fig. 7b and e; also see Fig. 2b).

Chemical zoning of fine-grained garnet in *Type 3* microstructures is analogous to that in *Type 2* aggregates discussed above (Fig. 7c and d). Coarse-grained fragments possess zoning similar to *Type 1* in that Ca and Y define four compositional domains, however the inner cores (Ca zone 1) exhibit a distinct 'patchy' distribution of Ca (Fig. 7c) and Y. Detailed inspection reveals a complex network of thin Ca/Y-depleted boundaries that separate larger areas of Ca/Y-enriched composition (Fig. 7d).

Microstructures 2-L1 3-1 (Fig. 7b and c), M1605-2-L3 6, and 2-L1- (Fig. 7e) are associated, respectively, with a decreasing relict size and increasing proportions of associated aggregate, and appear to represent various stages in a transition from *Type 1* to *Type 2*. Quantitative point analyses obtained from traverses across these relict porphyroclasts are in agreement with qualitative observations (Fig. 7g and h). In general, pyrope is rather homogeneous in all three microstructures, with concentrations of ~7–8% throughout the relict porphyroclasts. Profiles of spessartine progress from bell-shaped profiles with core concentrations

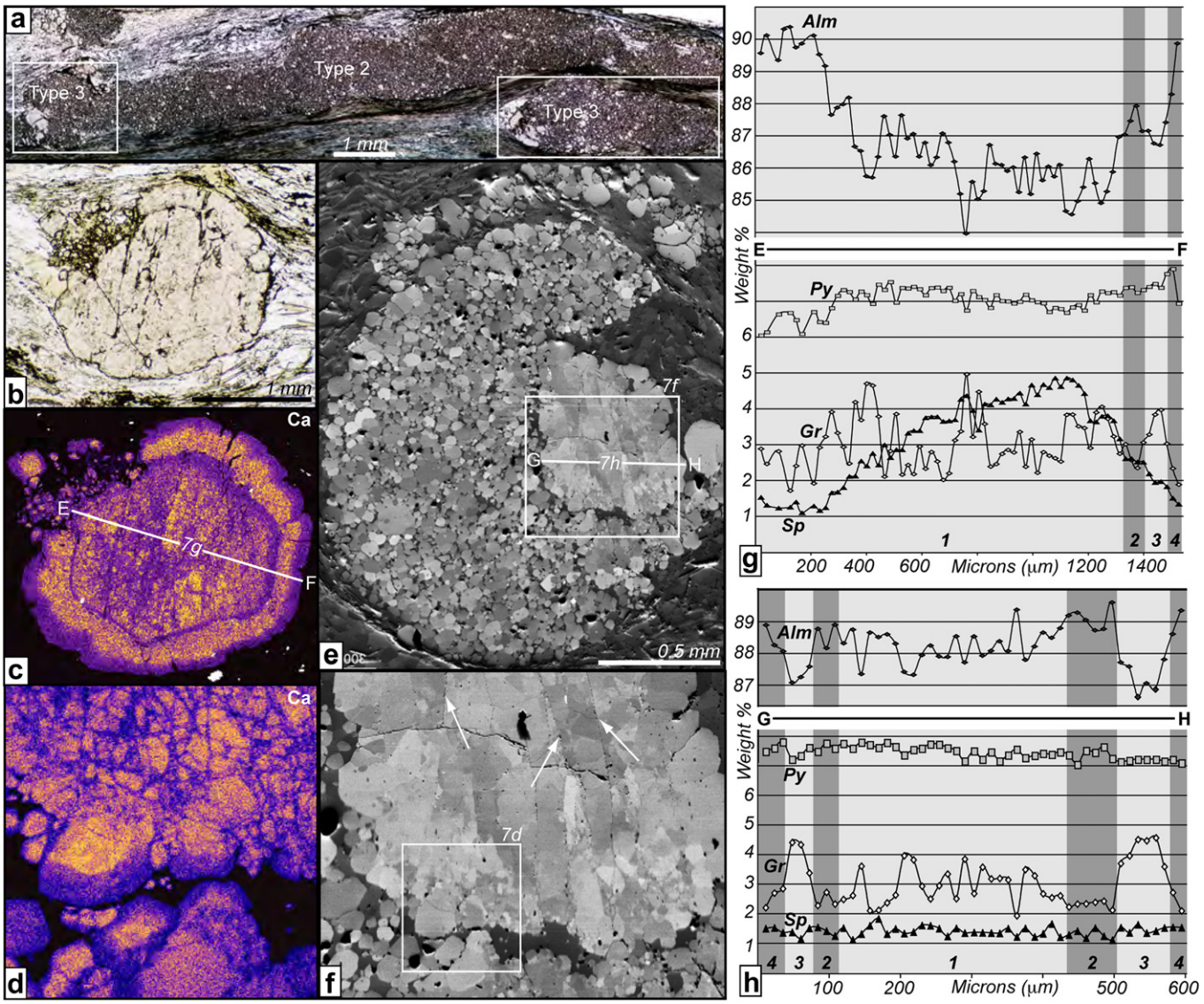

Fig. 7. *Type 3* transitional microstructures. (a) Photomicrograph illustrating intimate association and scale-dependence of garnet *Types 2* and *3*. *Type 3* porphyroclasts and associated aggregates connected by long *Type 2* aggregate. (b) Photomicrograph of sigma-type porphyroclast with minor associated aggregate. (c) Compositional X-ray map showing Ca growth zoning in garnet from (b). Notice four Ca zones in porphyroclast, similar to zoning in *Type 1* porphyroclast, but with a more depleted and erratic composition of inner core (Ca zone 1). Line E–F marks location of microprobe traverse shown in Fig. 7g. (d) Detailed Ca X-ray map of porphyroclast core shown in (f). Variable 'patchy' zoning similar to that shown in core in (c) is actually a complex network of thin Ca-depleted boundaries separating more broad areas of Ca-enriched composition (Ca zone 1). Boundaries appear to correspond to crystallographic boundaries in OC image (f). (e & f) OC images of *Type 3* microstructures. Notice lattice distortion, crystallographic boundaries, and subgrains similar in size to fine-grained aggregate garnet. Three sub-vertical fractures (arrows in (f)) are associated with crystallographic boundaries. Line G–H marks location of microprobe traverse shown in Fig. 9b. (g & h) Distribution of almandine, pyrope, grossular, and spessartine components taken along microprobe traverses across *Type 3* porphyroclasts. Varying shades of gray mark "Ca zones 1-4", as identified by X-ray mapping. (g) *Type 3* microstructure with high porphyroclast to aggregate proportion. (h) *Type 3* microstructure with low porphyroclast to aggregate proportion. Notice sharp compositional discontinuities in cores affect only Ca and Fe. Also notice drop in spessartine concentrations in 7g towards area of associated aggregate (see Fig. 7b and c) and lack of additional garnet growth (Ca zones 3 and 4), and the complete homogenization within the relatively small relict porphyroclast of 7h (see Fig. 7e).

>5% in the largest relicts with minor associated aggregate (Fig. 7g; compare to *Type 1* porphyroclasts in Fig. 3f and g), to completely homogenized compositions of >1% (Fig. 7h) in smallest relicts with relatively large proportions of aggregate. Grossular and almandine define erratic profiles within Ca zone 1 cores that range in composition from ~1–5% and ~84–89%, respectively (Fig. 7g and h). Note that the large variations of grossular in cores are completely balanced by an opposing variation in almandine. Conversely, grossular and almandine compositions remain stable in overgrowths (Ca zones 2 and 3) and rims (Ca zone 4), with each zone identifiable by a distinct chemistry (Fig. 7g and h). It should also be noted that toward areas where overgrowths and rims are apparently absent, there is in overall trend of depletion of all major elements, although most noticeable in the spessartine component (Fig. 7g).

OC imaging exposes considerable substructure and crystal lattice distortion within porphyroclast cores (Ca zones 1 and 2) that corresponds to the complex Ca/Y distributions in coarse-grained regions (Fig. 7d–f). Elongate, sub-vertical (orthogonal to the bulk foliation) domains are separated by crystallographic boundaries, some of which are associated with discrete fractures (Fig. 7f). Subgrain structures (≤25 μm) comparable in size to individual grains in aggregates are also prevalent in porphyroclasts, often concentrated along the linear crystallographic boundaries as well as margins that do not show significant garnet growth that produced Ca zones 3 and 4 (Fig. 7f). Fine-grained equant garnet is locally observed included in

porphyroclast rims (Ca zone 3), outside the regions of inner core substructures. There is a high concentration of substructure and lattice distortion developed within all *Type 3* porphyroclasts imaged in this study, and the amount of subgrain development appears to correspond proportionally to the state of transition from *Type 1* to *Type 2*. The same substructures that typify *Type 3* porphyroclasts (lattice distortion, low-angle boundaries, and subgrain development) are also found within small anhedral grains dispersed throughout aggregates.

5. EBSD: crystallographic orientation

Type 2 garnet microstructures have been examined by automated EBSD in order to test for a crystallographic preferred orientation (CPO) that could be related to macroscopic strain. Bulk CPO of individual microstructures was collected at step sizes greater than average individual grain sizes within the microstructure. Several microstructures were mapped in detail in order to establish spatial relationships between CPO, boundary misorientation, and substructure. In these cases, raw data were processed using the methodology of Prior et al. (2002): data are presented as one point per grain, with grains less than four times the step size removed. CPO's from detailed maps are presented below as lower hemisphere equal area plots of 1200 grains randomly selected from a larger dataset of individual grains within the microstructure. Pole figures were plotted and contoured using the program PFch5.app.sit (Mainprice: http://www.gm.univ-montp2.fr/PERSO/mainprice/).

5.1. Type 2 — aggregates

Bulk CPO's of *Type 2* microstructures have been collected from four separate aggregates in two specimens, with each microstructure having recorded various amounts of apparent accumulated strain. In order of increasing axial ratio: microstructure 2-L1-6 is a circular (~1:1) delta-shaped aggregate (Fig. 8a), ~1 mm in diameter; 2-L3-4 is a semi-elliptical (~2:1), delta-shaped, mm-sized aggregate (Fig. 8b; also see Fig. 4b); 2-L1-8 is an elongate (~3:1), sigma-shaped aggregate ~6 mm in length (Fig. 8c; also see Fig. 4a); 2-L3-1 is an asymmetrically-folded wing of fine-grained garnet extending off of a delta-shaped aggregate (Fig. 8d; also see Fig. 4b).

Each CPO is characterized by a maximum of {100} parallel to lineation, and a weaker girdle of {100} normal to foliation (Fig. 8). Preferred orientations of {110} and {111} are not as convincing. In all four cases, the CPO's are consistent and comprise a weak "fiber texture" in which all directions are rotated around one {100}, in this case parallel to lineation. It should also be noted that CPO intensity generally decreases with increasing axial ratio of the associated microstructure. Detailed grain boundary mapping of one aggregate (Fig. 9a) shows a predominance of high angles (>10°) of garnet-garnet grain boundaries, misoriented by random crystallographic axes (Fig. 9b). Neighbor- and random-pair misorientation angles match those of predicted random distributions, except for a small population of neighbor- and random-pairs at low angles (Fig. 9c). The proportional relationship between neighbor- and random-pair distributions implies that the low-angles are a function of the CPO (Wheeler et al., 2001).

5.2. Type 3 — transitions

Three *Type 3* transitional microstructures from two different specimens have been mapped in detail, each with varying proportions of aggregate and relict porphyroclast. 2-L3-6 is a sigma-shaped microstructure consisting of a millimeter-sized porphyroclast with relatively minor aggregate developed in one wing (Fig. 10a). In

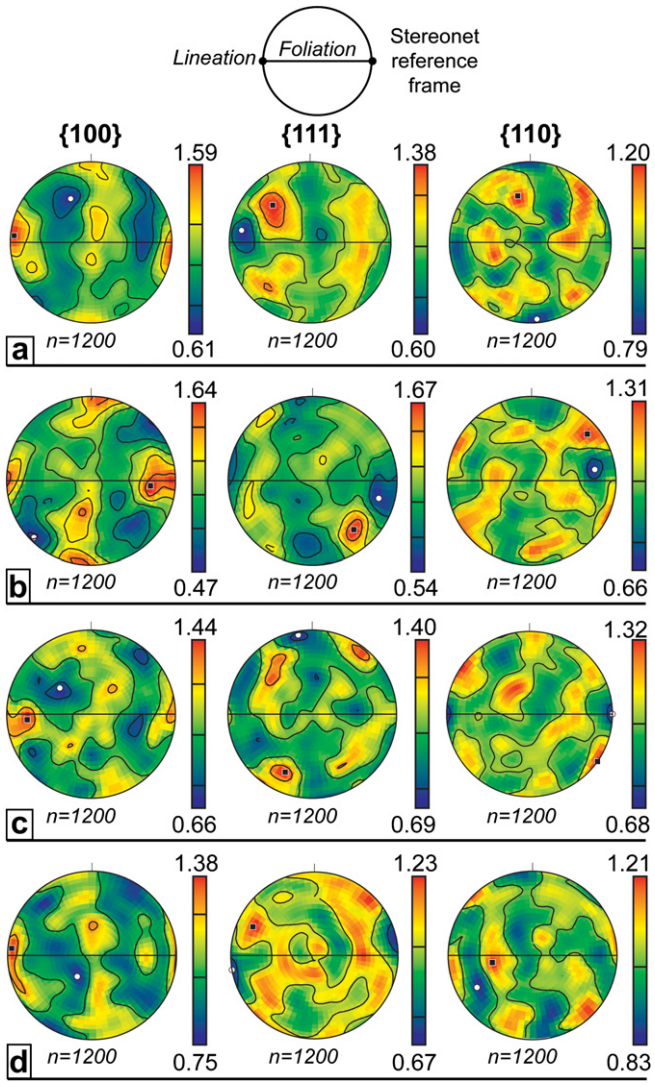

Fig. 8. Lower hemisphere equal area nets of 1200 random grains from *Type 2* aggregates, representing bulk CPO. Contours are in multiples of 0.25 times mean uniform distribution, with minima and maxima noted. Reference frame of plots is shown. Plots organized in order of increasing axial ratio of microstructure: (a) Sample 2-L1-6. (b) Sample 2-L3-4. (c) Sample 2-L1-8. (d) Sample 2-L3-1. Notice consistency of patterns throughout all samples, especially of {100} poles, although CPO intensity decreases slightly with increasing axial ratio.

microstructure 2-L1-9, two sub-millimeter-sized relicts occupy the regions adjacent to the sigma-shaped tails of quartz, while an approximately equal proportion of aggregate separates these two relicts (Fig. 10b). 2-L1-2 is a delta-shaped microstructure consisting predominantly of aggregate with one sub-millimeter-sized relict porphyroclast (Fig. 10c; also see Fig. 7e).

CPO of relict coarse-grained garnet porphyroclasts correspond to single crystal orientations, as would be expected for a single garnet porphyroclast (Fig. 10). CPO of associated fine-grained garnet within the same microstructure cluster around the same single crystal orientation as that of the coarse-grained garnet, although the pattern has been significantly weakened (Fig. 10). The degree of weakening in each CPO also corresponds to an increase in the proportion of aggregate to relict.

Grain boundaries within the aggregate are dominated by high angles (>10°), while coarse-grained porphyroclast substructures observed in OC images (boundaries and subgrains) correspond to predominantly low angles (Fig. 11a). Grain boundaries are

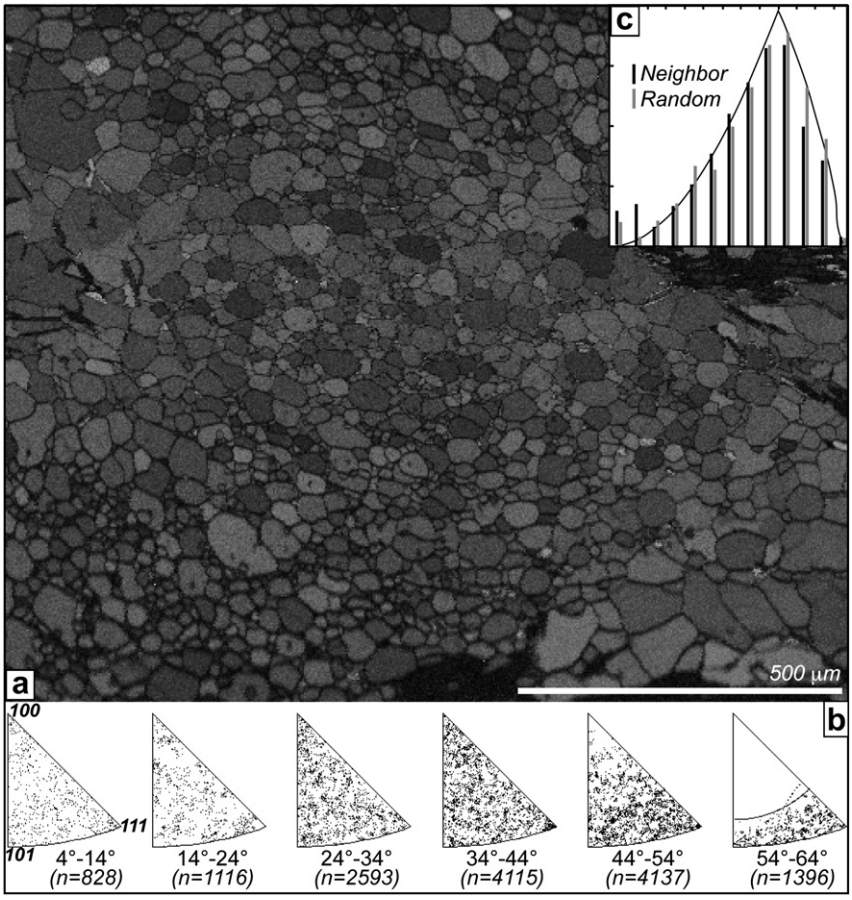

Fig. 9. (a) EBSD pattern quality map of portion of *Type 2* aggregate 2-L3 1 (2.5 μm step size). Grayscale of each pixel reflects precision of signal, where darker shades are of poorer quality and generally correspond to grain/phase boundaries. (b) Misorientation axis data for microstructure shown in a, plotted on inverse pole figures in 10° increments. (c) Frequency distribution of misorientation angles between pairs of neighboring (black) and randomly selected grains (gray) for microstructure shown in a. The line represents the expected distribution from a random CPO.

misoriented by random misorientation axes (Fig. 11b); however, the lower angle boundaries (≤24°) show a weak clustering along the {001}–{111} tie line of the inverse pole figure. Misorientation distributions show a high frequency of low-angle neighbor- and random-pair boundaries, while higher angle neighbor-pair and random-pair boundaries follow the theoretical random distribution (Fig. 11c). Notice that the majority of low-angle boundaries are confined to coarse-grained relict porphyroclasts, while the aggregates are typified by higher angles. It should also be noted that although internal deformation is widespread in relicts, it does not significantly alter the single crystal signature due to such small angles of misorientation.

6. Substructures

Intracrystalline substructure is widespread within both micron-scale garnet grains comprising aggregates of *Type 2* and *3* microstructures, and relict porphyroclasts that define *Type 3* microstructures. Detailed EBSD mapping and compositional X-ray mapping have been used to study the structural and chemical signature of the three distinct substructures, the results, of which, are presented below.

6.1. Inclusions

Small (5–15 μm), equant inclusion substructures are common within individual garnet grains from *Types 2* and *3* aggregate (see Fig. 4e). Faceted geometries of inclusion boundaries are revealed by OC imaging and detailed EBSD mapping. Some inclusions mapped do show similar orientations as their host crystal, but most inclusion-host microstructures show significant differences in orientation. Ca zoning of inclusions is similar to matrix crystals (Ca-enriched core, Ca-depleted rim), although Ca-depleted rims are locally absent.

6.2. Stacks

Sub-vertical impingement and 'stacking' of garnet crystals is a common substructure within the aggregates of *Types 2* and *3* microstructures (Fig. 12; also see Fig. 4e). The stacking axis is sub-vertical (parallel to pole to foliation) to steeply inclined, garnet-garnet grain boundaries normal to the stacking axis are curved, and garnet 'stacks' are frequently bounded by sub-vertical zones of quartz (Fig. 12). Detailed compositional mapping reveals elliptical Ca zoning of individual grains comprising stacks (Fig. 12e). Outer Ca-depleted rims are commonly thinned along grain boundaries normal to the stacking axis, compared to relatively thicker rims on boundaries parallel to the stacking axis. Complete truncation of Ca-depleted rims along stacked garnet boundaries is also observed, leading to juxtaposition of Ca-enriched cores against neighboring garnet grains (Fig. 12e). However, we observe no evidence of *new* material addition on stacking axis-parallel boundaries.

Strain analyses (via Fry method using GeoFryplots software by Holcombe: http://www.holcombe.net.au/software/rodh_software_downloads.htm#GeoFryPlots) of different regions of stacking substructures yield strain ellipse ratios ranging from 1.14 to 1.85,

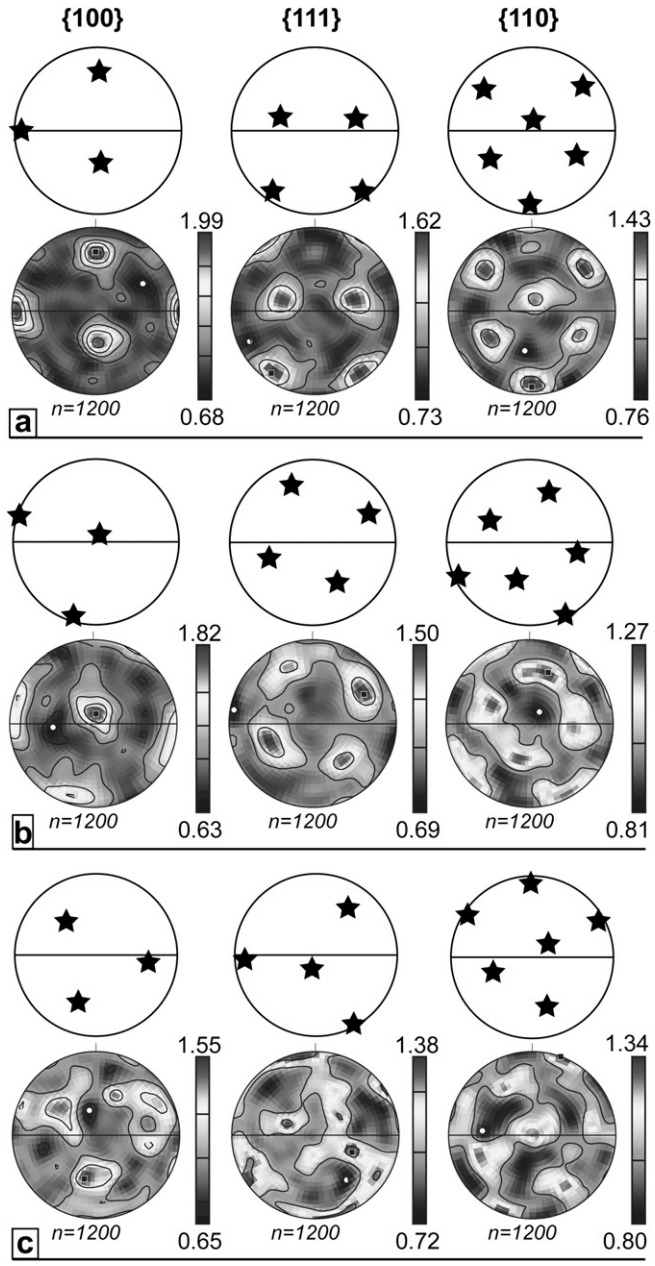

Fig. 10. Lower hemisphere equal area nets of 1200 random grains from *Type 3* microstructures, representing bulk CPO, and orientation of associated relict porphyroclast (stars); stereonet reference frame same as in Fig. 8. Although porphyroclasts show considerable substructure and deformation, maxima of crystal axes correspond to a single crystal orientation. Plots organized in order of increasing proportions of aggregate comprising the microstructure: (a) Sample 2-L3-6. (b) Sample 2-L1-9. (c) Sample 2-L1-2. Notice correlation of porphyroclast and fine-grained aggregate CPO's, and weakening of CPO with increasing proportion of aggregate.

which increase with the axial ratio of the larger-scale host microstructure (Fig. 12f). Long axes of calculated strain ellipses are approximately coincident to the stacking direction. This indicates that garnet crystals were exposed to flattening strains sometime after their development, and stacking was part of this deformation.

6.3. Fragments

Irregularly shaped, anhedral grains within the fine-grained aggregate are noticeably larger (usually >50 μm) than faceted grains and show considerable lattice distortion, low-angle boundaries, and subgrain development typical of dislocation creep processes (Fig. 13). However, the similarity of these substructures to *Type 3* relict substructures make it reasonable to assume that these grains are smaller correlatives distributed throughout the aggregates. Although fragments are observed in both *Type 2* and *Type 3* aggregate, there exists a wider range of size in *Type 3* microstructures, further supporting their relationship with the larger *Type 3* relicts.

7. Garnet compositions

Textural observations presented above imply that *Type 2* aggregates evolved from original *Type 1* garnet porphyroclasts along a path characterized by *Type 3* transitional microstructures. OC imaging suggests that this microstructural evolution is a result of intracrystalline deformation (low-angle boundaries, subgrains, and fracturing) localized within certain porphyroclasts, dividing original garnet porphyroclasts into *Type 1* and *Type 3* microstructures. The increase in relative proportions of aggregate grains with decreasing relict porphyroclast size and with increase of porphyroclast deformation, and the comparable size of subgrains within relict porphyroclasts and individual aggregate garnet grains, all indicate that aggregate garnet evolved from *Type 3* porphyroclasts by deformation. Although textural evidence for the derivation of aggregate garnet by deformation is extensive, the composition of garnet defining each microstructure must corroborate the interpretation in order to rule out any alternate reaction and nucleation processes.

X-ray mapping clearly reveals the presence of four distinct compositional zones within *Type 1* porphyroclasts marked by Ca (see Fig. 3), and quantitative point analyses show that each zone is characterized by a distinct chemistry (Fig. 14a and b; also see Fig. 3). Although estimated temperatures of peak staurolite-grade metamorphism (Spear et al., 2002; Berg and Moecher, 2005) were sufficient for the homogenization of zoning profiles, residence time at these temperatures must have been insufficient, resulting in incomplete homogenization of major elements and preservation of original growth zoning (e.g., Chakraborty and Ganguly, 1992; Ayres and Vance, 1997; Carlson and Schwarze, 1997; Carlson, 2006). The simplest interpretation for the preserved compositional growth zoning is a two-phase growth history comprised of prograde nucleation (Ca zones 1 and 2), followed by retrograde growth (Ca zones 3 and 4). As such, original growth zoning preserved by almandine and grossular components may be used as a standard for comparison of garnet compositions from *Type 2* and *3* microstructures (Fig. 14).

Compositional zoning within relict porphyroclasts of *Type 3* microstructures is analogous to that of *Type 1* porphyroclasts, characterized by the same four Ca zones; however, *Type 3* porphyroclasts contain an additional characteristic of irregular, sharp compositional discontinuities within cores (Ca zone 1). The presence of low-angle boundaries, subgrains, and fractures along these compositional discontinuities suggest that deformation was involved in producing the zoning patterns. Although the mechanism that produced the compositional variations will be discussed in detail below, it can be seen that the progression of *Type 3* microstructures toward *Type 2* microstructures has an effect on garnet composition (Fig. 14c–e). With increasing deformation (and decreasing size of relict grain), almandine and grossular components within cores (Ca zone 1) show an increasing degree of scatter, becoming chemically indistinguishable from subsequent overgrowth compositions (Ca zones 2–4; Fig. 14c and d), and eventually stabilizing at a composition that defines a range between that of Ca zones 3 and 4 (Fig. 14e). The stabilized composition range of the

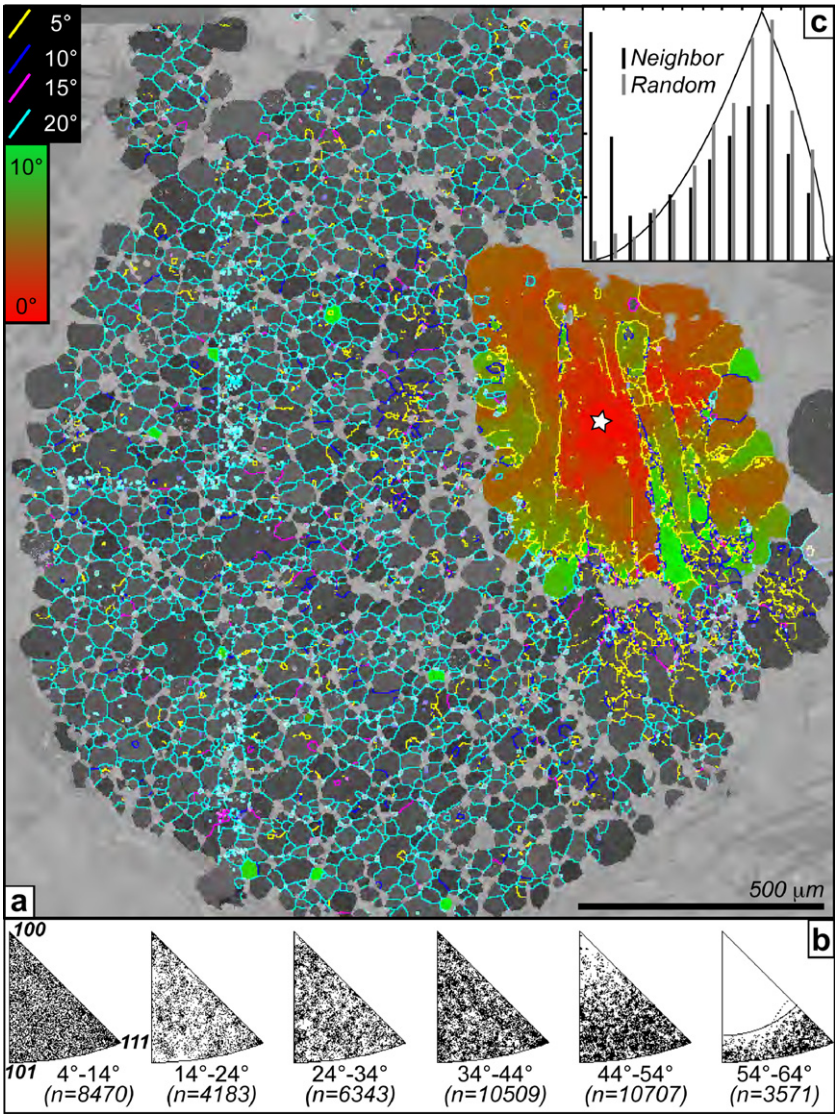

Fig. 11. (a) Boundary map superimposed on EBSD pattern quality map of *Type 3* aggregate and porphyroclast 2-L1-2 (2.5 μm step size), with omission of grains less than four times the step size. Grain boundary misorientations are color-coded according to misorientation angle (see legend). Texture component map of large porphyroclast shows pixels that are misoriented less than 10° relative to specified point (star), where increasing misorientation angles are shown by transition from red (0° misorientation) to green (10° misorientation). Vertical lines on left side of map are caused by a slight mismatch associated with a stitching error. (b) Misorientation axis data for microstructure shown in (a), plotted on inverse pole figures in 10° increments. (c) Frequency distribution of misorientation angles between pairs of neighboring (black) and randomly selected grains (gray) for microstructure shown in (a). The line represents the expected distribution from a random CPO. (For interpretation of the references to color in this figure legend, the reader is referred to the web version of this article).

most evolved/deformed *Type 3* relict porphyroclast cores is the same as that defined by cores of individual aggregate garnet grains (Fig. 14f), strongly suggesting that aggregate grains were derived directly from relicts.

7.1. Effects of diffusion

Although temperatures were sufficiently high for volume diffusion of major cations, it was assumed in the preceding discussion that residence times at such temperatures were insufficient for complete major element homogenization (other than Mg) in *Type 1* porphyroclasts (e.g., Chakraborty and Ganguly, 1992; Ayres and Vance, 1997; Carlson and Schwarze, 1997; Carlson, 2006). However, it has been shown that intracrystalline deformation may enhance major cation diffusion rates, even at temperatures well below the closure temperature for volume diffusion (e.g., Kramar et al., 2001; Reddy et al., 2006). In addition to the complex Ca-depleted/Fe-enriched compositional zoning in cores of *Type 3* relicts, deformation has created a network of fast-diffusion pathways by lowering length scales of diffusivity (e.g., Kramar et al., 2001; Reddy et al., 2006). In the present study, the effects of such fast-diffusion pathways are most apparent in the distribution of the spessartine component, although Mg, Fe, and Ca vaguely show the same trends. As *Type 3* porphyroclasts are increasingly altered and the overall grain size decreases, the original bell-shaped profile of spessartine (see Fig. 7g and h and compare with Fig. 3f and g) is progressively depleted and eventually homogenized at ~1% (see Fig. 7h). Post-deformation garnet growth appears to have effectively sealed fast-diffusion pathways in the largest/least deformed *Type 3* porphyroclasts, as original bell-shaped profiles are partially preserved in areas surrounded by thick overgrowths (Ca zones 3 and 4; see Fig. 7g and location of profile in Fig. 7c).

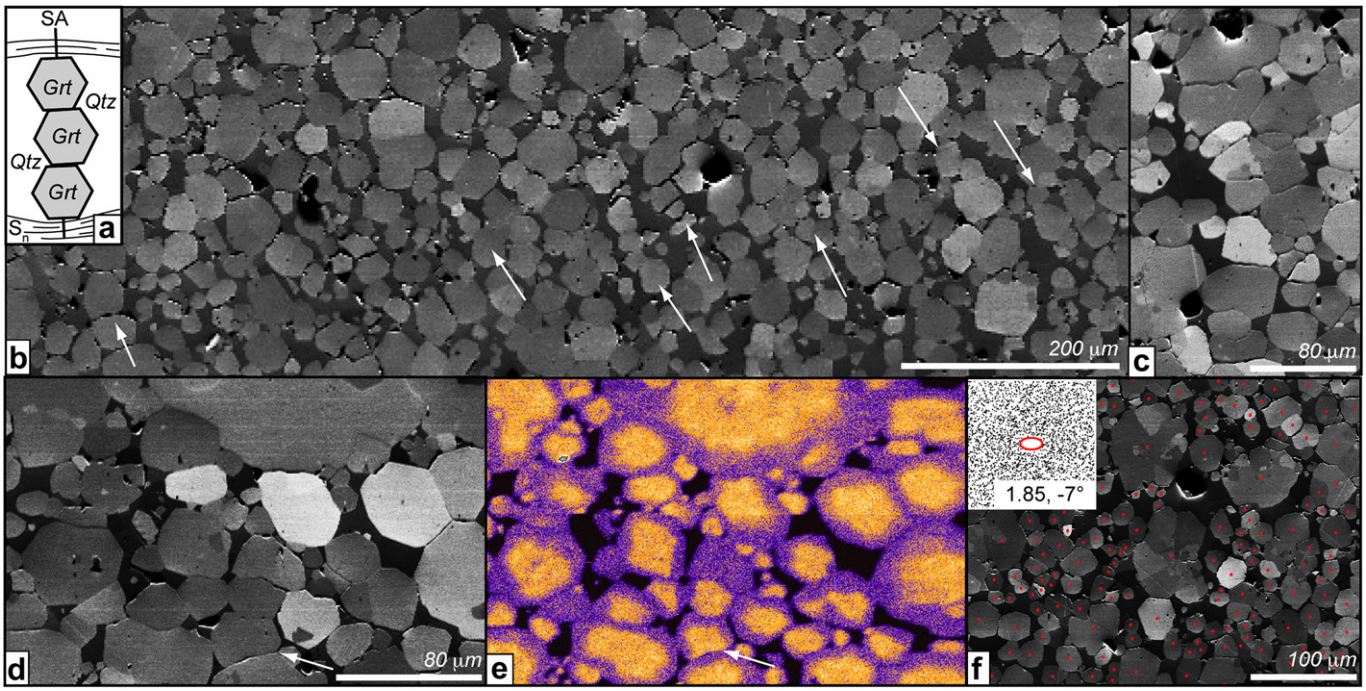

Fig. 12. (a) Schematic diagram of 'stacking' substructure found in garnet aggregates. A sub-vertical column of garnet crystals is bounded by sub-vertical columns of quartz, and defined by a stacking axis (SA) oriented approximately orthogonal to the foliation (Sn). (b) OC image showing sub-vertical stacking (arrows) within aggregate. Notice that sub-vertical columns of quartz parallel the sides many garnet stacks. (c & d) Detailed OC images of 'stacking' substructures. Notice slightly curved geometry of stacked grain boundaries, and elliptical grain shapes with long axes normal to stacking direction. (e) Detailed Ca X-ray map of 'stack' substructures shown in (d). Arrows in (d) and (e) point to the same grain boundary. Notice juxtaposition of Ca-enriched core of top grain against Ca-depleted overgrowth/boundary of bottom grain. (f) OC image of one 'stacking' substructure image used for Fry analysis (shown in top left). Calculated strain ellipse (1.85) and orientation (−7°) approximates shape and orientation of stacked grains in OC image.

8. Garnet substructure and CPO development

Dislocation creep and dynamic recrystallization processes commonly produce strong CPO's of the deforming mineral (e.g., quartz, olivine, plagioclase, calcite, pyroxene). Garnet CPO's presented here are weak. However, in cubic minerals, such as garnet and pyrite, crystal plastic deformation predominantly results in weak to random orientations (e.g., Mainprice et al., 2004; Storey and Prior, 2005; Barrie et al., 2007; Bestmann et al., 2008). This is at least in part due to the multiplicity of active slip systems in minerals with cubic symmetry, and the relative rigidity of garnet compared with common matrix components (quartz, mica, clinopyroxene, amphibole, etc.). There also exists the possibility of competing CPO-weakening deformation mechanisms such as grain boundary sliding (e.g., Jiang et al., 2000; Bestmann and Prior, 2003; Storey and Prior, 2005; Mehl and Hirth, 2008; Skemer and Karato, 2008).

The CPO's of *Type 2* polycrystalline garnet aggregates are consistent throughout multiple hand specimens, and symmetric with respect to tectonic fabric (foliation and lineation). However, data from *Type 3* transitional microstructures indicates that fine-grained aggregate garnet mimics associated coarse-grained garnet porphyroclast orientations. In both types of microstructures, CPO's are non-random, and their existence can be explained by two contrasting possibilities. First, the CPO's are the direct result of tectonic deformation that lead to the development of the present mylonitic fabric, as well as the preferred orientation of fine-grained aggregate garnet. This hypothesis would assume then, that *Type 2* microstructures and CPO's are more evolved than *Type 3*. Second, the CPO's are host-controlled, where orientations of pre-existing coarse-grained garnet have been inherited by younger fine-grained garnet. We first consider several mechanisms for the former option.

8.1. Dislocation creep and recovery of aggregate garnet

Dislocation glide and climb, recovery, and dynamic recrystallization can all lead to CPO development; however, evidence for the activity of these processes in aggregate garnet grains is lacking. Irregularly shaped grains are commonly scattered throughout both *Type 2* and *Type 3* aggregates, and exhibit the types of substructures that can lead to a CPO. However, based on textural similarities with *Type 3* relict porphyroclasts and the higher frequency of observed occurrence within *Type 3* aggregate, these grains must be fragments of deformed porphyroclasts and not representative of the deformation affecting younger aggregate garnet grains.

8.2. Coalescence of aggregate garnet

Equant, faceted inclusion substructures are observed within individual aggregate garnet grains, although their occurrence is not widespread. Based on the lack of additional deformation and substructure within the host garnet, and the range of misorientation data between inclusion and host, we interpret these substructures as evidence for limited coalescence among aggregate garnet crystals. The similarity of compositional zoning in individual aggregate garnet grains and inclusion substructures, require that the coalescence process followed formation of aggregate garnet. Spiess et al. (2001) interpret CPO's of aggregates as forming by surface energy driven rotations during coalescence. The resulting CPO's approximate single crystal orientations, do not share the symmetry elements of the deformation fabrics, and differ significantly from aggregate to aggregate. The CPO's we present do no support surface energy driven rotations. Lack of such rotations is not problematic; Okamoto and Michibayashi (2006) provide evidence for coalescence without rotation due to lower temperatures. In our study, post peak metamorphic temperatures during the final stages of deformation are

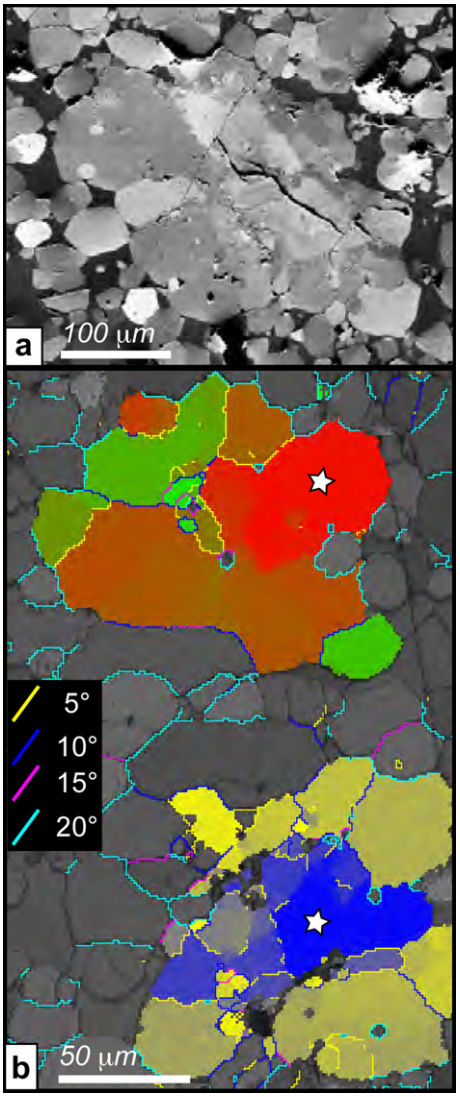

Fig. 13. (a) OC image of anhedral fragment within aggregate, showing considerable lattice distortion, boundaries, and subgrains. (b) Detailed boundary map overlaid on EBSD pattern quality map with texture components of two separate grains (1 μm step size; different from a). Notice similarity to *Type 3* porphyroclast substructures in Fig. 7.

estimated at 450–550 °C (peak metamorphism 550–625 °C; Spear et al., 2002; Berg and Moecher, 2005) and are unlikely to facilitate surface energy driven rotations rapid enough to modify CPO's (Spiess et al., 2001).

8.3. Grain boundary sliding of aggregate garnet

Although there is no indication of significant intracrystalline deformation by dislocation creep processes within the majority of aggregate grains, aggregates could have deformed by other means. Terry and Heidelbach (2004) showed that grain boundary sliding was the primary deformation mechanism for ~10 μm garnet in an eclogite facies shear zone. Storey and Prior (2005) and Bestmann et al. (2008) both indicated that as dynamic recrystallization progressed and the development of individual grains increased, primary deformation mechanisms switched to grain boundary sliding.

In aggregates of both *Type 2* and *3* microstructures, there is abundant evidence of physical interaction among neighboring grains (i.e., grain boundary sliding), in the form of sub-vertical impingement and stacking of individual garnet grains within the aggregate. The sub-vertical arrangement of individual grains within stacking structures suggests that aggregate garnet grains were subjected to flattening strains sometime after their development, consistent with the calculated strains. Deformation by grain boundary sliding would also help explain the random misorientation axes and angles (see Figs. 9 and 11).

Grain boundary sliding requires an accommodation mechanism, such as frictional sliding and dilatation (Sammis, 2001), dislocation creep (Gifkins, 1991, 1994), or diffusion creep (Ashby and Verrall, 1973; Gifkins, 1973, 1976). Elliptical grain shapes, grain size sensitive deformation, elliptical compositional zoning, truncation of zoning, and curved grain boundaries are all evidence for deformation by grain boundary diffusion creep (coble creep, pressure solution). The lack of garnet growth on boundaries parallel to the stacking axis suggests that material was transported from the aggregate via diffusive mass transfer. Volume diffusion of Ca would not be expected at these temperatures (e.g., Chakraborty and Ganguly, 1992; Ayres and Vance, 1997; Carlson and Schwarze, 1997; Carlson, 2006) and is consistent with the preservation of growth zoning. Additionally, the similarity of grain shape axial ratios and ratios calculated with the Fry method, suggest that flattening of the aggregate was primarily accommodated through grain boundary sliding by diffusion creep (pressure solution).

Sub-vertical stacking due to flattening would also require that the intervening quartz matrix be translated laterally in order for garnet grains to impinge vertically. In order to accommodate deformation within both garnet and quartz, aggregates must have stretched laterally in addition to being flattened. Sub-vertical columns of quartz that parallel garnet stacks (see Fig. 12a and b) agree with this interpretation. Within this context, diffusive mass transfer and precipitation or grain boundary sliding could account for quartz deformation, however, we have no direct constraints.

Grain boundary sliding accompanying diffusion creep is a CPO-weakening mechanisms (e.g., Jiang et al., 2000; Bestmann and Prior, 2003). However, contact between strongly faceted crystals, with facets being crystallographically controlled, could counteract the randomization of grain boundary sliding, and possibly account for the observed *Type 2* CPO's. Individual aggregate grains are predominantly characterized by faceted geometries, with most facets corresponding to {112} and {110} faces. In this case, any physical process (e.g., impingement and rotation) that would lead to stacking of {110} or {112} facet planes should produce CPO characterized by {110} or {112} maxima parallel to the stacking axis (pole to foliation). As such, these stacks cannot give rise to a {100} maximum parallel to lineation (normal to stacking axis/pole to foliation) observed in the bulk CPO's.

Stacking structures are clearly a result of sub-vertical flattening strains, which also correlate to the degree of deformation of the entire host microstructures as recorded by their axial ratios. However, the monoclinic symmetry of garnet microstructures (sigma- and delta-type asymmetric porphyroclasts, asymmetric folds), in addition to the overall fabric of the mylonitic rock, suggests that the bulk kinematic framework was likely dominated by a non-coaxial component of deformation. This may be explained by deformation partitioning within a multi-component rock where more competent domains accommodate coaxial strains (e.g., Menegon et al., 2008). Nevertheless, the stacking still represents an additional complication rather than a primary CPO generation mechanism, explaining the relationship between decreasing CPO intensity with increasing evolution of *Type 3* (increasing proportions of aggregate to relict porphyroclast) and *Type 2* (increasing axial ratios of the aggregate) microstructures.

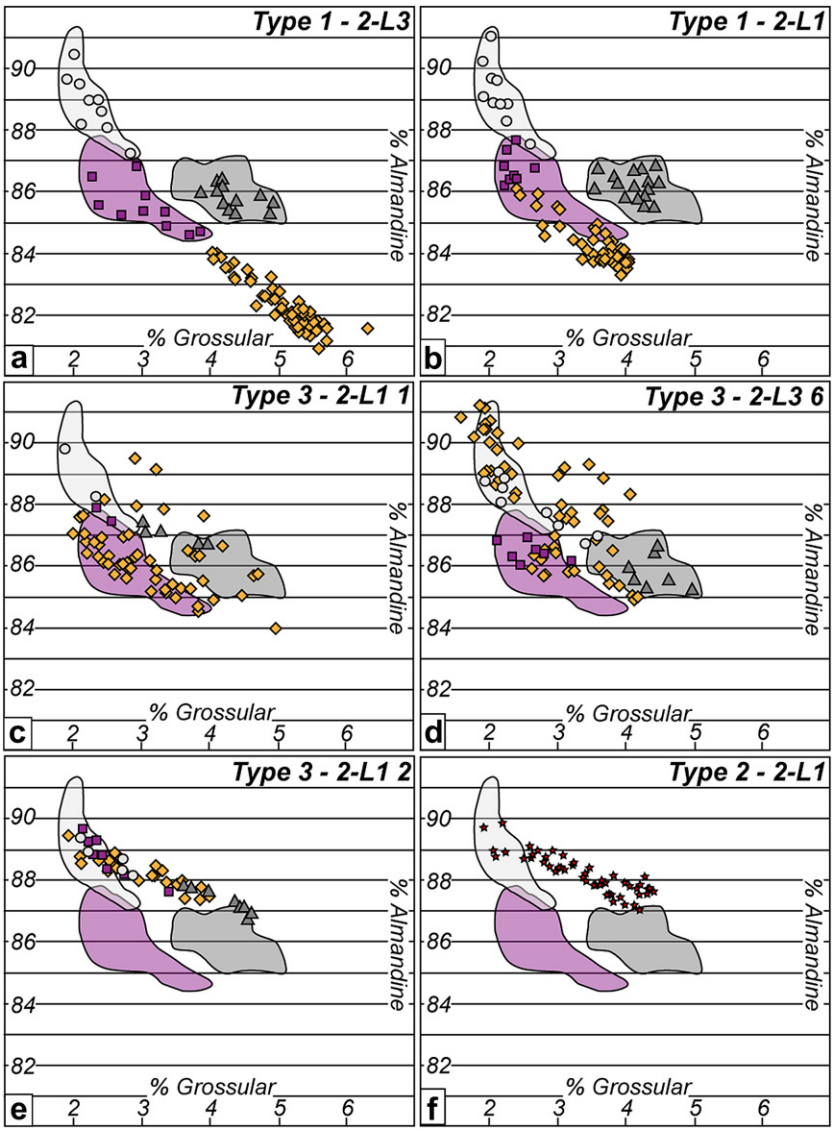

Fig. 14. Plots of grossular vs. almandine. (a & b) *Type 1* porphyroclasts. Notice that each of the four "Ca zones" identified in X-ray mapping is chemically distinct from one another. Orange diamonds: core-Ca zone 1; purple squares: overgrowth-Ca zone 2; dark gray triangles: overgrowth-Ca zone 3; light gray circles: rims-Ca zone 4. Note that the purple, dark gray, and light gray areas in all figures (a–f) represent the complete range of each zone observed within all *Type 1* porphyroclasts. (c, d, & e) *Type 3* porphyroclasts arranged by decreasing size of relict porphyroclast, and increasing ratio of aggregate to relict porphyroclast. Notice the growing scatter of core-Ca zone 1 compositions as *Type 3* microstructures progress (c & d), which eventually leads to a completely new apparent core composition (f). Also notice that although Ca zones 3 and 4 lose almandine, they are still chemically distinct from one another, while the 'new' core composition spans this range. (f) Individual aggregate garnet grain compositions (same as Fig. 6). Notice the similarity of garnet compositions of aggregate garnet grain in (f) and the core of an evolved *Type 3* porphyroclast in (e). (For interpretation of the references to color in this figure legend, the reader is referred to the web version of this article).

8.4. Inherited CPO of aggregate garnet

There is little evidence to support a model of transitional *Type 2* CPO development as a function of the most recent tectonic deformation. While grain boundary sliding did accommodate significant flattening strains within garnet aggregates during this youngest phase of deformation, it did not generate the observed CPO's. Therefore, CPO's and present microstructures must be consequences of inheritance and subsequent tectonic modification. Crystallographic orientations of new minerals can be influenced by several mechanisms: (1) epitaxial growth, where nucleation of new minerals on older ones is controlled by mutual lattice alignment (Spiess et al., 2007; Padrón-Navarta et al., 2008); (2) oriented nucleation within a stress field (Kamb, 1959; Passchier and Trouw, 1998); (3) lattice alignment by grain rotation (Spiess et al., 2001; Wheeler et al., 2001; Prior et al., 2002; Dobbs et al., 2003); (4) orientation inheritance of recrystallized grains from a host microstructure. There is no indication that aggregate garnet originated by any nucleation and growth process, such as (1) and (2). Lattice alignment by rotation in order to reduce grain boundary surface energy (3) is not considered by reasons outlined previously. Compositional similarities between relict porphyroclasts and aggregate garnet, and intracrystalline heterogeneities associated with relict porphyroclasts constitute evidence that supports an early phase of crystal-plastic deformation, consistent with aggregate garnet genesis and orientation inheritance (4).

8.4.1. Dislocation creep and recovery of Type 3 porphyroclasts

Observed lattice distortion, prevalence of low-angle boundaries, and subgrain development in porphyroclasts are evidence for dislocation creep and recovery processes, and subgrains are indeed

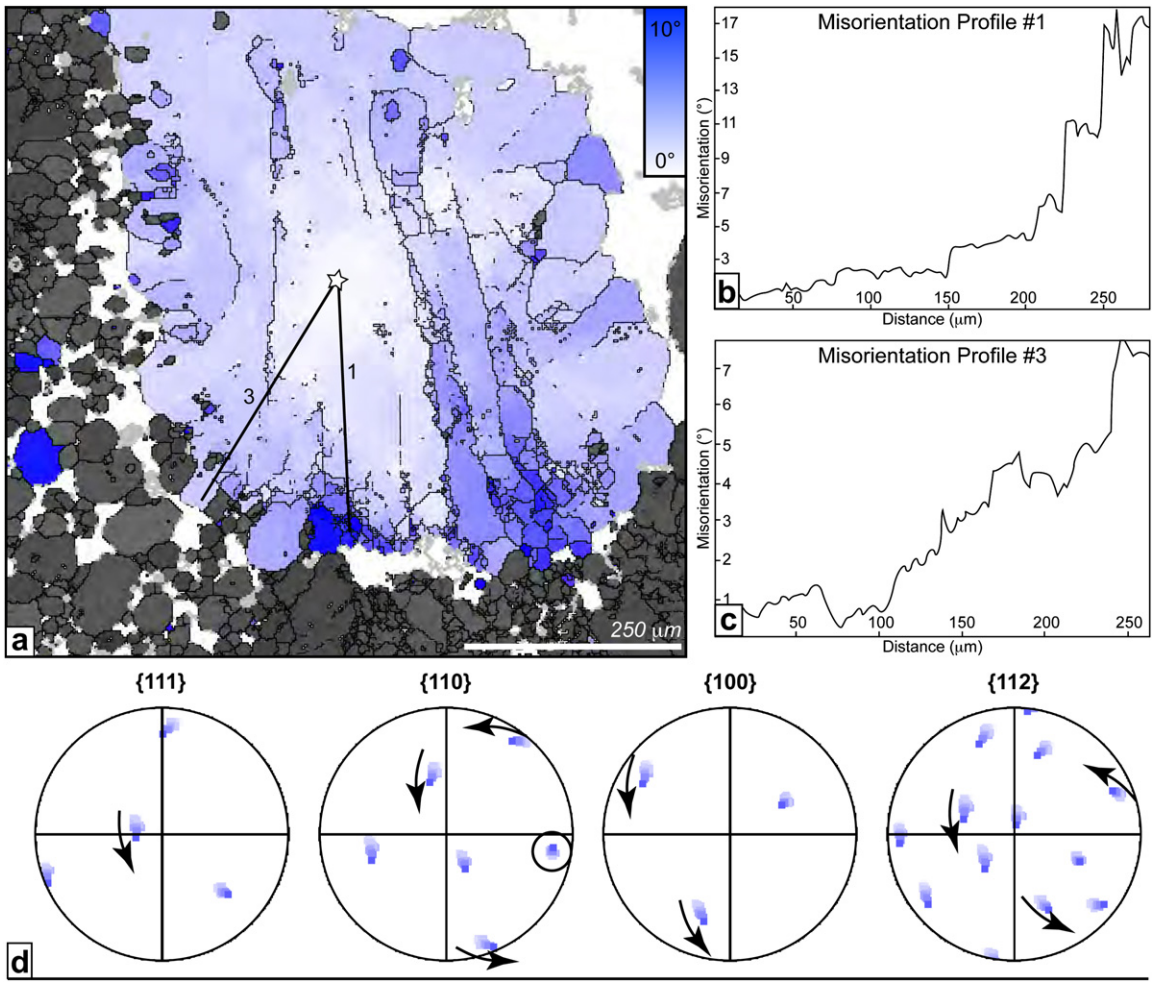

Fig. 15. *Type 3* porphyroclast and substructures, as shown in Fig. 11. (a) Texture component map and locations of misorientation profile traverses 1 and 3 shown in (b) and (c), respectively. Notice large increase in misorientation angles in profiles 1 and 3 toward porphyroclast margins and areas of abundant subgrains. (d) Stereonet of {100}, {110}, {111}, and {112} directions along misorientation profile traverse 1. Color-coding of stereonet corresponds to texture component of porphyroclast and illustrates the counter-clockwise dispersion around a distinct {110} axis. (For interpretation of the references to color in this figure legend, the reader is referred to the web version of this article).

equivalent in size to individual aggregate garnet grains (Fig. 15). Profiles of misorientation angles relative to specified points (Fig. 15b and c) show an increase in misorientation angle from subdomain centers toward porphyroclast margins and areas of pervasive subgrain development. Garnet orientations are dispersed around distinct crystallographic rotation axes across low-angle boundaries (Fig. 15d), and subgrains are often associated with these structures, both dependable indicators of dislocation creep and recovery processes (Lloyd and Freeman, 1991; Lloyd et al., 1997; Boyle et al., 1998; Prior et al., 2002; Bestmann and Prior, 2003; Storey and Prior, 2005; Bestmann et al., 2008). A simple interpretation for observed garnet CPO's would involve a mixture of slip systems with a <100> slip vector (<100>{100}, <100>{011}) to give <100> maxima on the lineation with no clear maximum on the pole to foliation, although confirmation would require a more detailed examination.

8.4.2. Fracturing and chemical segregation of Type 3 porphyroclasts

There is a clear spatial overlap of fractures, low-angle boundaries, and subgrains with the erratic compositional zoning preserved in *Type 3* relict cores. The arrangement of Ca-enriched (Fe-depleted) subdomains surrounded by thin Ca-depleted (Fe-enriched) zones appears as a healed fracture network at first glance, and fracture truncations of compositional domains are present, though rare. It is thus tempting to suggest a fracture mechanism to explain the zoning patterns and steep compositional gradients of Ca and Fe, especially since fractures are only present in *Type 3* relict cores and must be related to deformation. However, this type of process would not explain the relatively unchanged Mg and Mn concentrations. The clear dispersions around crystallographic axes across low-angle boundaries also suggests that fracturing alone does not adequately explain these microstructures, as critical and sub-critical fractures are not strongly controlled by garnet crystallography, nor are likely to produce idiomorphic garnet grains (Prior, 1993). Although fracturing may be linked with plastic deformation (Trepmann and Stöckhert, 2002; Storey and Prior, 2005), our evidence shows that dislocation creep and recovery processes are the predominant mechanisms for this phase of deformation.

Chemical segregation along intracrystalline boundaries is commonly observed in metallic alloys, semi-conductors, and ceramics (e.g., Bernardini, 1998; Ross et al., 2001; Wynblatt et al., 2003), and presents an alternative explanation of garnet zoning patterns. Plastic deformation in solid-solutions (such as garnet) can result in a preferential segregation of one end member over another in zones of lattice distortion in order to recover from stress. Storey and Prior (2005) invoked segregation as an active process associated with amphibolite facies garnet deformation and recrystallization, while Prior et al. (2000) and Matthews et al.

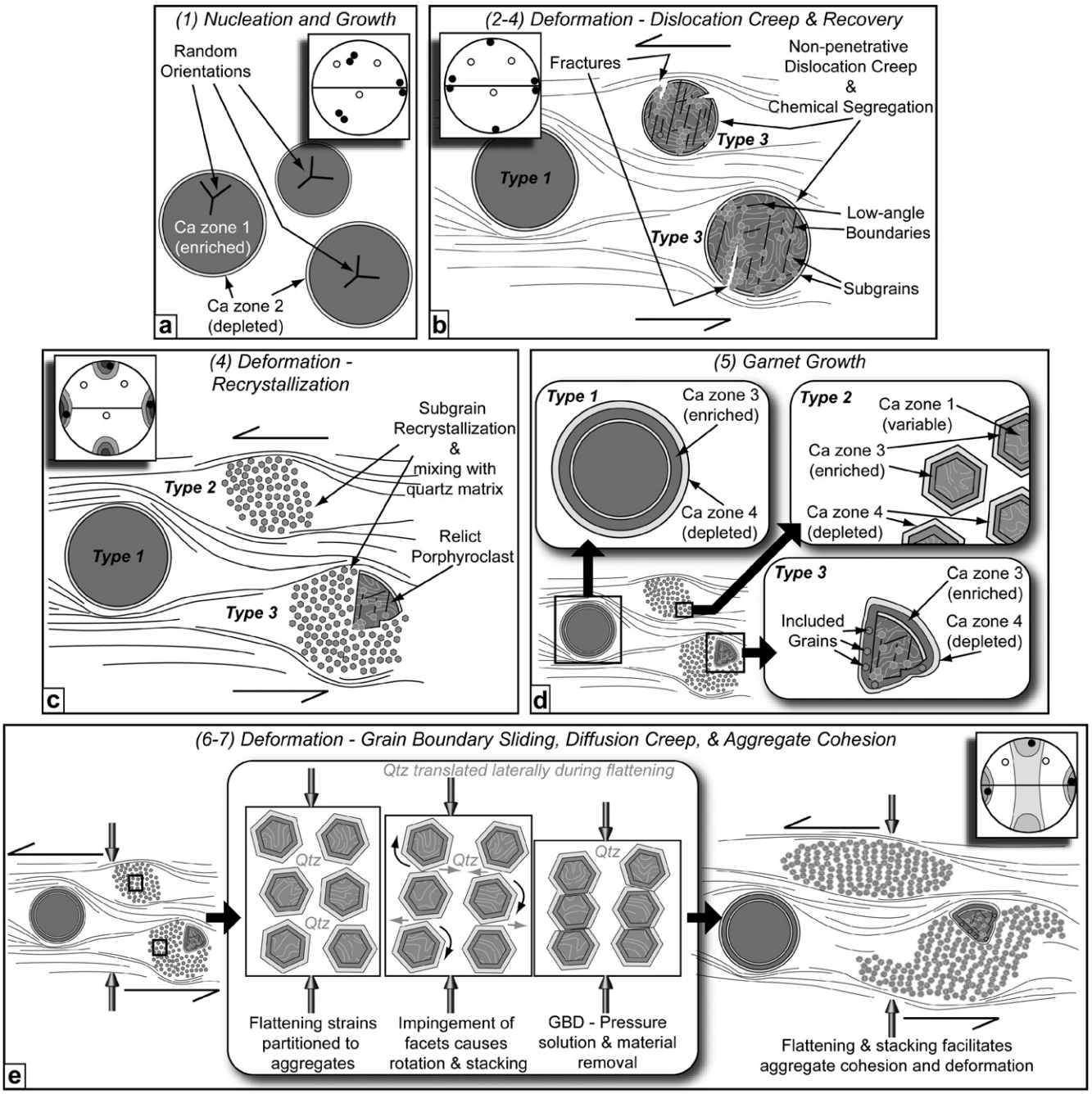

Fig. 16. Conceptual model of garnet microstructure and CPO evolution (see text for detailed discussion) showing initial nucleation and growth (a), early, non-penetrative crystal plastic deformation (b & c), additional growth (d), and final deformation and tectonic modification (e). Inset diagrams are equal area lower hemisphere plots of *Types 1* (white circles) and *3* (black circles) porphyroclasts, and recrystallized aggregates (contours). GBD, grain boundary diffusion.

(1992) also reported chemical differences along subgrain boundaries, although these were not interpreted as effects of chemical segregation. In the present study, compositional variations of *Type 3* porphyroclast cores are characterized by the depletion of ~1–2% Ca and enrichment of ~1–2% Fe along low-angle boundaries, while Mg and Mn are relatively unaffected. This pattern cannot be a result of modification by volume diffusion, even if temperatures were sufficient, but instead must be explained as the consequence of chemical segregation associated with the recovery of *Type 3* porphyroclasts. In this case, relatively large Ca ions were removed from sites within areas of high lattice distortion, replaced and chemically balanced by smaller Fe, likely facilitated by short-range vacancy diffusion (Storey and Prior, 2005).

8.4.3. Recrystallization

The observations that subgrains appear to increase in proportions as *Type 3* relicts are progressively deformed by dislocation creep, subgrains are similar in size to neighboring aggregate garnet grains, and that aggregate garnet grains are chemically identical to deformed *Type 3* porphyroclast cores are robust indications that aggregate garnet has formed by subgrain recrystallization (e.g., Storey and Prior, 2005; Bestmann et al., 2008). Recrystallization of *Type 3*

porphyroclasts would also require that recrystallized grains become mixed with surrounding matrix phases upon detachment from the host garnet porphyroclast. Although recrystallized aggregate garnet has maintained a bulk CPO that matches the original porphyroclast orientation, the signature has been weakened (see Figs. 8 and 10) and is likely, at least partially, a result of a mixing process with surrounding quartz. The necessary mixing with quartz and the weakening of CPO is most consistent with a grain boundary sliding process. Dynamic recrystallization leading to phase mixing by sliding is commonly reported (Bestmann and Prior, 2003; Storey and Prior, 2005; Bestmann et al., 2008), and seems most plausible in this setting as well. Textural and compositional relationships of all microstructures demonstrate this phase of deformation and recrystallization followed initial prograde garnet growth, but preceded late retrograde garnet growth, consistent with conditions of similar styles of deformation (e.g., Storey and Prior, 2005; Bestmann et al., 2008).

9. Conceptual model and summary

Fig. 16 presents a conceptual model that best explains the data presented herein. Although the bulk of this work was aimed at the substructures within the polycrystalline aggregates and associated CPO (see 5–7 below), we presented observations that constrain initial garnet parageneses and early deformation (see 1–4 below).

(1) Prograde amphibolite facies metamorphism is recorded in *Types 1* and *3* garnet porphyroclast euhedral to subhedral cores, by enriched cores and thin depleted overgrowths, Ca zones 1 and 2, respectively. CPO's of single crystals are random. At this stage, there is no distinction between garnets that will remain *Type 1* and those that will evolve to *Type 3* and *Type 2* garnet microstructures, other than perhaps their orientations (Fig. 16a).
(2) Grains oriented for glide on active slip systems during dislocation creep undergo non-penetrative deformation (Fig. 16b). Deformation partitioning results in dislocation creep of *Type 3* porphyroclasts, while *Type 1* behave as rigid porphyroclasts. CPO develops in *Type 3* garnets with {100} parallel to lineation and normal to foliation (Fig. 16b).
(3) *Type 3* garnets recover through the development of low-angle boundary networks, and develop into fractures. Chemical segregation is part of the recovery process, leading to rearrangement of distorted lattice by depletion of Ca and enrichment of Fe through vacancy diffusion (Fig. 16b).
(4) Small (10–20 μm) subgrains become concentrated along low-angle boundaries and fractures (Fig. 16b), eventually resulting in complete detachment and generation of 'aggregate' matrix garnet (Fig. 16c). Recrystallized grains inherit orientation and compositional zoning of *Type 3* host porphyroclast. CPO is weakened with increasing recrystallization, a result of detached garnet grains mixing with surrounding quartz matrix. Continued deformation results in complete recrystallization of *Type 3* porphyroclasts and formation of *Type 2* polycrystalline aggregates. Deformation and recrystallization enhance diffusivity properties of garnet.
(5) Garnet growth continues along the retrograde path (Fig. 16d). Overgrowths on *Types 1* and *3* porphyroclasts record Ca zones 3 (Ca-enriched) and 4 (Ca-depleted). Garnet growth is identical for aggregate garnet, however, Ca zone 3 is rarely recognized in X-ray maps because of their Ca-enriched cores. Aggregate garnet within *Types 2* and *3* microstructures undergoes local coalescence and inclusion within neighboring grains.
(6) Deformation continues into lower amphibolite to upper greenschist facies conditions (Fig. 16e). Aggregates deform internally by flattening, although overall asymmetries of microstructures also require a component of non-coaxial strain. Original CPO's are further weakened, but neither rotated nor erased. The decrease in temperature and reduced grain size likely initiates the change in predominant garnet deformation mechanism from dislocation creep to diffusion creep.
(7) Deformation proceeds by diffusion creep, requiring boundary sliding (Fig. 16e). Stacking of faceted garnet crystals and grain boundary diffusion accommodates predominantly flattening strains. Ca-depleted compositions (Ca zone 4) are removed from grain boundaries in the shortening direction by pressure solution and transported away from the aggregate. Interstitial quartz between garnet grains is transported laterally as stacking progresses.

Microstructural and EBSD data establish that *Types 1*, *2* and *3* garnet represent a microstructural continuum, where *Type 3* microstructures are transitional between 'undeformed' *Type 1* porphyroclast and 'deformed' *Type 2* aggregate end members. Substructures found in *Type 3* porphyroclast cores are most consistent with an early phase of non-penetrative dislocation creep and recovery close to the peak of staurolite-grade metamorphism. *Type 2* aggregates evolved from continued dislocation creep and recovery processes (chemical segregation and subgrain recrystallization) of *Type 3* porphyroclasts, while *Type 1* porphyroclasts were excluded from this deformation. The absence of any textural differences between any garnet microstructure type suggests that deformation and microstructural development is an effect of strain partitioning, rather than an association with external features (S–C domains, shear bands, mineralogical and chemical heterogeneities observed in the matrix) as observed by Storey and Prior (2005). It is presently unclear why this deformation was confined only to *Type 3* garnets. Evidence for partitioning may have been reconstituted and erased during progressive deformation, although this is entirely speculative. Alternatively, it seems most plausible that initial orientations of *Type 3* porphyroclasts may have been conducive for deformation by the active slip system(s). Given the overall transpressional symmetry and progressive deformation of the high strain zone (Massey and Moecher, 2008), it seems entirely possible that *Type 1* porphyroclasts may not have rotated into this orientation while at suitable PT conditions for this style of dislocation creep and recovery. Measuring and comparing orientations of *Type 1* porphyroclasts and *Type 3* relict porphyroclasts could test this hypothesis, however, the number of thin sections needed for a statistically significant number of measurements (several hundred from each type of microstructure) was not possible in this study. Further examination is necessary to substantiate these ideas.

The CPO's of *Type 2* aggregates are weak, however, it is the fact that the {100} consistently forms a maxima parallel to lineation and a girdle normal to foliation/lineation throughout multiple samples that make these convincing as a bulk CPO associated with tectonic deformation. These fabrics are unlike any modeled by Mainprice et al. (2004), which were based on the <111>{110} slip system, or those presented from natural settings by Kleinschrodt and Duyster (2002), Ji et al. (2003), and Storey and Prior (2005). Bulk CPO's of *Type 2* and *3* aggregates are products of inheritance from deformation (early dislocation creep, recovery, and recrystallization) of a precursor garnet porphyroclast, rather than deformation within the aggregates themselves (grain boundary sliding/facet-controlled 'stacking', limited coalescence and amalgamation). The relationship between porphyroclast orientation and aggregate CPO in *Type 3* microstructures, the presence of small 'fragments' of the parent porphyroclast dispersed throughout aggregates, and the non-random distribution of low-angle neighbor- and random-pair misorientation angle distributions in both *Type 2* and *3* aggregates support this interpretation.

Microstructural, chemical, and crystallographic data presented in this paper also demonstrate the significance of strain accommodation within microcrystalline garnet aggregates by grain boundary sliding and grain boundary diffusion creep at lower amphibolite to upper greenschist facies. Terry and Heidelbach (2004) and Storey and Prior (2005) suggest that grain boundary sliding within garnet aggregates resulted in a weakening process, allowing fine-grained garnet to mix with surrounding syn-tectonic phases and play an equal role in defining fabric. In contrast, garnet aggregates examined in this study seem to have been restrained from mechanical mixing with matrix phases other than quartz, by remaining relatively cohesive, preserving original porphyroclast shapes and CPO's. Although monoclinic fabric elements and microstructures (S–C fabric, delta- and sigma-type asymmetric porphyroclasts and aggregates, etc.) suggest a non-coaxial component of deformation, aggregates must have accommodated a large proportion of coaxial flow in order to account for aggregate substructures and the lack of rotation of inherited CPO's. Coaxial flattening and compaction during the final stages of deformation appears to have facilitated aggregate cohesion, ultimately resulting in a strain hardening process.

In a more generalized sense, this study supplements the growing body of evidence for garnet deformation by crystal plastic mechanisms spanning a wide range of thermobarometric conditions (Ji and Martingole, 1994; Kleinschrodt and McGrew, 2000; Kleinschrodt and Duyster, 2002; Prior et al., 2000, 2002; Storey and Prior, 2005; Bestmann et al., 2008). Although the polycrystalline aggregates studied here are unusual (however see: Okamoto and Michibayashi, 2006), these microstructures are mineralogically comparable to more common garnetiferous rocks (e.g., peridotites) and could possibly provide insight into possible deformation mechanisms within the deep crust and mantle. Conversely, the variously shaped garnet porphyroclasts are quite common, implying the potential for considerably more occurrences of garnet deformation than what has been reported. It is also evident that intracrystalline deformation may have a profound influence on garnet chemistry during the recovery process (chemical segregation), as well as post-deformation diffusion at conditions not expected for volume diffusion. The pervasive substructures and associated chemical heterogeneities would never have been identified without EBSD methods, and further illustrate the power and importance of these methods to any study that even partially relies upon an understanding of garnet.

Acknowledgments

We wish to thank Tom Walker for help with microprobe analyses. We are also appreciative of M. Herwegh and G. Pennacchioni for their thorough reviews, which greatly enhanced the manuscript.

References

Ashby, M.F., Verrall, R.A., 1973. Diffusion accommodated flow and superplasticity. Acta Metallurgica 21, 149–163.
Ayres, M., Vance, D., 1997. A comparative study of diffusion profiles in Himalayan and Dalradian garnets: constraints on diffusion data and the relative duration of the metamorphic events. Contributions to Mineralogy and Petrology 128, 66–80.
Barrie, C.D., Boyle, A.P., Prior, D.J., 2007. An analysis of the microstructures developed in experimentally deformed polycrystalline pyrite and minor sulphide phases using electron backscatter diffraction. Journal of Structural Geology 29, 1494–1511.
Bell, T.H., Johnson, S.E., 1989. Porphyroblast inclusion trails: the key to orogenesis. Journal of Metamorphic Geology 7, 279–310.
Bell, T.H., Kim, H.S., 2004. Preservation of Acadian deformation and metamorphism through intense Alleghanian shearing. Journal of Structural Geology 26, 1591–1613.
Bernardini, J., 1998. Segregation and grain boundary diffusion in metals and elemental semi-conductors. Defect and Diffusion Forum 156, 49–50.
Berg, C.A., Moecher, D.P., 2005. Apparent oxygen isotope equilibrium during progressive foliation development and porphyroblast growth in metapelites: implications for stable isotope and conventional thermometry. Journal of Metamorphic Geology 23, 471–487.
Bestmann, M., Prior, D.J., 2003. Intragranular dynamic recrystallization in naturally deformed calcite marble: diffusion accommodated grain boundary sliding as a result of subgrain rotation recrystallization. Journal of Structural Geology 25, 1597–1613.
Bestmann, M., Habler, G., Heidelbach, F., Thoni, M., 2008. Dynamic recrystallization of garnet and related diffusion processes. Journal of Structural Geology 30, 777–790.
Boyle, A.P., Prior, D.J., Banham, M.H., Timms, N.E., 1998. Plastic deformation of metamorphic pyrite: new evidence from electron-backscatter diffraction and forescatter orientation–contrast imaging. Mineralium Deposita 34, 71–81.
Carlson, W.D., 2006. Rates of Fe, Mg, Mn, and Ca diffusion in garnet. American Mineralogist 91, 1–11.
Carlson, W.D., Schwarze, E.T., 1997. Petrologic significance of prograde homogenization of growth zoning in garnet: an example from the Llano Uplift. Journal of Metamorphic Geology 15, 631–644.
Chakraborty, S., Ganguly, J., 1992. Cation diffusion in aluminosilicate garnets: experimental determination in spessartine-almandine diffusion couples, evaluation of effective binary diffusion coefficients, and applications. Contributions to Mineralogy and Petrology 111, 74–86.
Daniel, C.G., Spear, F.S., 1998. 3-Dimensional patterns of garnet nucleation and growth. Geology 26, 503–506.
Deer, W.A., Howie, R.A., Zussmann, J., 1992. An Introduction to the Rock Forming Minerals. Longman, Harlow. 696pp.
Dobbs, H.T., Peruzzo, L., Seno, F., Spiess, R., Prior, D.J., 2003. Unraveling the Schneeberg garnet puzzle: a numerical model of multiple nucleation and coalescence. Contributions to Mineralogy and Petrology 146, 1–9.
Getty, S.R., Gromet, L.P., 1992. Geochronological constraints on ductile deformation, crustal extension, and doming about a basement-cover boundary, New England Appalachians. American Journal of Science 292, 398–420.
Gifkins, R.C., 1973. Superplasticity, creep and grain-boundary sliding. Scripta Metallurgica 7, 27–33.
Gifkins, R.C., 1976. Grain-boundary sliding and its accommodation during creep and superplasticity. Metallurgical Transactions A—Physical Metallurgy and Materials Science 7, 1225–1232.
Gifkins, R.C., 1991. Ductility and strain-rate control mechanisms in superplasticity. Scripta Metallurgica et Materialia 25, 1397–1400.
Gifkins, R.C., 1994. Grain-boundary participation in high temperature deformation: a historical review. Materials Characterization 32, 59–77.
Ji, S.C., Martignole, J., 1994. Ductility of garnet as an indicator of extremely high-temperature deformation. Journal of Structural Geology 16, 985–996.
Ji, S.C., Saruwatari, K., Mainprice, D., Wirth, R., Xu, Z., Xia, B., 2003. Microstructures, petrofabrics and seismic properties of ultra high-pressure eclogites from Sulu region, China: implications for rheology of subducted continental crust and origin of mantle reflections. Tectonophysics 370, 49–76.
Jiang, Z.T., Prior, D.J., Wheeler, J., 2000. Albite crystallographic preferred orientation and grain misorientation distribution in a low-grade mylonite: implications for granular flow. Journal of Structural Geology 22, 1663–1674.
Kamb, W.B., 1959. Theory of preferred orientation development by crystallisation under stress. Journal of Geology 67, 153–170.
Kleinschrodt, R., McGrew, A., 2000. Garnet plasticity in the lower continental crust: implications for deformation mechanisms based on microstructures and SEM-electron channeling pattern analysis. Journal of Structural Geology 22, 795–809.
Kleinschrodt, R., Duyster, J.P., 2002. HT-deformation of garnet: an EBSD study on granulites from Sri Lanka, India and the Ivrea Zone. Journal of Structural Geology 24, 1829–1844.
Kohn, M.J., Catlos, E.J., Ryerson, F.J., Harrison, T.M., 2001. Pressure–temperature–time path discontinuity in the Main Central thrust zone, central Nepal. Geology 29, 571–574.
Kramar, N., Cosca, M.A., Hunziker, J.C., 2001. Heterogeneous $^{40}Ar^{*}$ distributions in naturally deformed muscovite: in situ UV-laser ablation evidence for microstructurally controlled intragrain diffusion. Earth and Planetary Science Letters 192, 377–388.
Li, L., Long, H., Raterron, P., Weidner, D., 2006. Plastic flow of pyrope at mantle pressure and temperature. American Mineralogist 91, 517–525.
Lloyd, G.E., Freeman, B., 1991. SEM electron channeling analysis of dynamic recrystallization in a quartz grain. Journal of Structural Geology 13, 945–953.
Lloyd, G.E., Farmer, A.B., Mainprice, D., 1997. Misorientation analysis and the formation and orientation of subgrain and grain boundaries. Tectonophysics 279, 55–78.
Mainprice, D., Nicolas, A., 1989. Development of shape and lattice preferred orientations: application to the seismic anisotropy of the lower crust. Journal of Structural Geology 11, 175–190.
Mainprice, D., Bascou, J., Cordier, P., Tommasi, A., 2004. Crystal preferred orientations of garnet: comparison between numerical simulations and electron backscattered diffraction (EBSD) measurements in naturally deformed eclogites. Journal of Structural Geology 26, 2089–2102.
Massey, M.A. and Moecher, D.P., 2008. Dextral transpression and heterogeneous ductile extrusion of the Monson orthogneiss, New England Appalachians. In: Van Balen, Mark (ed.), New England Intercollegiate 100th Annual Conference, Westfield, Massachusetts.
Matthews, M., Harte, B., Prior, D.J., 1992. Mantle garnets: a cracking yarn. Geochimica et Cosmochimica Acta 56, 2633–2642.

Mehl, L., Hirth, G., 2008. Plagioclase preferred orientation in layered mylonites: evaluation of flow laws for the lower crust. Journal of Geophysical Research-Solid Earth 113. doi:10.1029/2007JB005075.
Menegon, L., Pennacchioni, G., Heilbronner, R., Pittarello, L., 2008. Evolution of quartz microstructure and c-axis crystallographic preferred orientation within ductilely deformed granitoids (Arolla unit, Western Alps). Journal of Structural Geology 30, 1332–1347.
Moecher, D.P., Wintsch, R.P., 1994. Deformation-induced reconstitution and local resetting of mineral equilibria in polymetamorphic gneisses: tectonic and metamorphic implications. Journal of Metamorphic Geology 12, 523–538.
Moecher, D.P., 1999. The distribution, style, and intensity of Alleghanian metamorphism in south-central New England: petrologic evidence from the Pelham and Willimantic domes. Journal of Geology 107, 449–471.
Okamoto, A., Michibayashi, K., 2006. Misorientations of garnet aggregate within a vein: an example from the Sanbagawa metamorphic belt, Japan. Journal of Metamorphic Geology 24, 353–366.
Padrón-Navarta, J.A., Garrido, C.J., Sanchez-Navas, A., Tommasi, A., Sanchez-Vizcaino, V.L., Gomez-Pugnaire, M.T., Hussain, S.S., 2008. Oriented growth of garnet by topotactic reactions and epitaxy in high-pressure, mafic garnet granulite formed by dehydration melting of metastable hornblende-gabbronorite (Jijal Complex, Kohistan Complex, north Pakistan). Journal of Metamorphic Geology 26, 855–870.
Passchier, C.W., Trouw, R.A.J., 1998. Micro-tectonics. Springer, New York. 289pp.
Pattison, D.R.M., Tracy, R.J., 1991. Phase-equilibria and thermobarometry of metapelites. Reviews in Mineralogy 26, 105–206.
Prior, D.J., 1993. Subcritical fracture and associated retrogression of garnet during mylonitic deformation. Contributions to Mineralogy and Petrology 113, 545–556.
Prior, D.J., Trimby, P.W., Weber, U.D., Dingley, D.J., 1996. Orientation contrast imaging of microstructures in rocks using forescatter detectors in the scanning electron microscope. Mineralogical Magazine 60, 859–869.
Prior, D.J., Wheeler, J., Brenker, F.E., Harte, B., Matthews, M., 2000. Crystal plasticity of natural garnet: new microstructural evidence. Geology 28, 1003–1006.
Prior, D.J., Wheeler, J., Peruzzo, L., Spiess, R., Storey, C., 2002. Some garnet micro structures: an illustration of the potential of orientation maps and misorientation analysis in microstructural studies. Journal of Structural Geology 24, 999–1011.
Read, H.H., 1970. Rutley's Elements of Mineralogy. Thomas Murbo, London. 560pp.
Reddy, S.M., Timms, N.E., Trimby, P., Kinny, P.D., Buchan, C., Blake, K., 2006. Crystal-plastic deformation of zircon: a defect in the assumption of chemical robustness. Geology 34, 257–260.
Robinson, P., Tucker, R.D., Bradley, D., Berry IV, H.N., Osberg, P.H., 1998. Paleozoic orogens in New England, U.S.A. Geologiska Foreningen i Stockholm Forhandlingar (GFF) 120, 119–148.
Ross, I.M., Rainforth, W.M., McComb, D.W., Scott, A.J., Brydson, R., 2001. Grain boundary segregation in Al2O3 doped 3Y-TZP ceramics, electron microscopy and analysis 2001. Institute of Physics Conference Series, 299–302.
Rutter, E.H., Casey, M., Burlini, L., 1994. Preferred crystallographic orientation development during the plastic and superplastic flow of calcite rocks. Journal of Structural Geology 16, 1431–1447.
Sammis, C.G., 2001. Materials science issues in the Earth and Planetary sciences. Progress in Materials Science 46, 231–247.
Schmid, S.M., Casey, M., 1986. Complete fabric analysis of some commonly observed quartz c-axis patterns. In: Hobbs, B.E., Heard, H.C. (Eds.), Mineral and Rock Deformation: Laboratory Studies – The Paterson Volume. American Geophysical Union, Geophysical Monograph, pp. 263–286.
Skemer, P., Karato, S.I., 2008. Sheared lherzolite xenoliths revisited. Journal of Geophysical Research-Solid Earth 113. doi:10.1029/2007JB005286.
Solar, G.S., Brown, M., 2001. Deformation partitioning during transpression in response to Early Devonian oblique convergence, northern Appalachian orogen, USA. Journal of Structural Geology 23, 1043–1065.
Spear, F.S., 1992. Thermobarometry and P–T paths from granulite facies rocks: an introduction. Precambrian Research 55, 201–207.
Spear, F.S., Selverstone, J., 1983. Quantitative P–T paths from zoned minerals: theory and tectonic applications. Contributions to Mineralogy and Petrology 83, 348–357.
Spear, F.S., Kohn, M.J., Cheney, J.T., Florence, F., 2002. Metamorphic, thermal, and tectonic evolution of central New England. Journal of Petrology 43, 2097–2120.
Spiess, R., Peruzzo, L., Prior, D.J., Wheeler, J., 2001. Development of garnet porphyroblasts by multiple nucleation, coalescence and boundary misorientation-driven rotations. Journal of Metamorphic Geology 19, 269–290.
Spiess, R., Groppo, C., Compagnoni, R., 2007. When epitaxy controls garnet growth. Journal of Metamorphic Geology 25, 439–450.
Storey, C.D., Prior, D.J., 2005. Plastic deformation and recrystallization of garnet: a mechanism to facilitate diffusion creep. Journal of Petrology 46, 2593–2613.
Terry, M.P., Heidelbach, F., 2004. Superplasticity in garnet from eclogite facies shear zones in the Haram Gebbro, Haramsøya, Norway. Geology 32, 281–284.
Trepmann, C.A., Stockhert, B., 2002. Cataclastic deformation of garnet: a record of synseismic loading and postseismic creep. Journal of Structural Geology 24, 1845–1856.
van Staal, C.R., 2006. Pre-Carboniferous metallogeny of the Canadian Appalachians; Mineral Deposits of Canada, Natural Resources Canada (http://gsc.nrcan.gc.ca/mindep/synth_prov/appalachian/index_e.php).
Voegele, V., Ando, J.I., Cordier, P., Liebermann, R.C., 1998a. Plastic deformation of silicate garnets I: high-pressure experiments. Physics of the Earth and Planetary Interiors 108, 305–318.
Voegele, V., Cordier, P., Sautter, V., Sharp, T.G., Lardeaux, J.M., Marques, F.O., 1998b. Plastic deformation of silicate garnets II: deformation microstructures in natural samples. Physics of the Earth and Planetary Interiors 108, 319–338.
Wheeler, J., Prior, D.J., Jiang, Z., Spiess, R., Trimby, P.W., 2001. The petrological significance of misorientations between grains. Contributions to Mineralogy and Petrology 141, 109–124.
Whitney, D.L., Seaton, N.C.A., 2010. Garnet polycrystals and the significance of clustered crystallization. Contributions to Mineralogy and Petrology 160, 591–607.
Wynblatt, P., Rohrer, G.S., Papillon, F., 2003. Grain boundary segregation in oxide ceramics. Journal of the European Ceramic Society 23, 2841–2848.